TROPOMI observations of SO_2 emissions from the January 2020 Taal Eruption and other volcanoes across the Philippine Mobile Belt and Indonesian Sangihe/Halmahera Arcs

A Thesis Submitted to the University of Manchester for the Degree of Master of Philosophy
In the Faculty of Science and Engineering

February 2023

Ellie-May Redfern
Department of Earth and Environmental Science

Contents

Abstract

Quantifying SO_2 emissions from explosive eruptions and quiescent volcanic degassing provides insights into the eruption dynamics and magmatic processes associated with a specific volcano. Satellite remote sensing has paved the way for accessible SO_2 imagery; however, the raw imagery provides only masses, and further analysis is needed to produce the SO_2 flux and plume height data which aids in filling the gap that is required for understanding explosive eruption events. SO_2 fluxes and plume heights were quantified from TROPOMI analysed with the newly developed PlumeTraj toolkit during the January 2020 Taal eruption and specific quiescent and eruptive volcanoes across the Philippine Mobile Belt and Indonesian Sangihe and Halmahera arc systems. An SO_2 flux data series with injection time (UTC), injection altitude (km), and SO_2 emission (kg s^{-1}) were created which allowed the calculation of the average and peak Mass Eruption Rate (MER) and sulphur content ($S_{content}$) within the pre- and post- eruptive magma. An average monthly SO_2 output (t day^{-1}) was calculated using the averaging approach applied against the method for TROPOMI with PlumeTraj for Taal, Mayon, Kanlaon, Karangetang and Dukono. The results from the averaging approach allowed a visual insight into the trend of degassing which coincided with the observational reports and activity seen from the volcanoes during the same period. The results from the January 2020 SO_2 time flux series showed that both the MER and $S_{content}$ within the pre-eruptive magma was higher ($S_{content}$ equal to 550.37 ppm; MER equal to 5.55 x 10^6 kg s^{-1}) during the main eruptive phase on 12/01/20 than the post-eruptive magma ($S_{content}$ equal to 91.77 ppm; MER equal to 4.33 x 10^6 kg s^{-1}) on 13/01/20. The results also reveal three separate injection altitudes at 2.5 km, 12.8 km, and 18 km. I found that the difference in SO_2 flux, $S_{content}$, and MER coincided with the observational reports from the Philippine Institute of Volcanology and Seismology (PHIVOLCS). From these findings I suggest the introduction of a singular sulphur-rich magmatic intrusion prior to the start of the eruption causing five SO_2 flux injections seen across both days, the possible cause for the differing injection altitudes. This study highlights the applications of TROPOMI using additional software to refine the quantification of SO_2 from explosive and passively degassing volcanic systems.

Acknowledgements

First and foremost, I would like to express my deepest appreciation to Prof Mike Burton and Dr Brendan McCormick Kilbride for their support and feedback throughout my journey. I could also not have taken this journey without the help of Dr Cat Hayer and Dr Benjamin Esse for their invaluable patience and time with helping me understand absolutely everything when it comes to PlumeTraj and Python. I would also like to extend my sincere thanks to the University of Manchester Counselling Service, with special thanks to Ella White who has supported me throughout the majority of my time at Manchester.

I am incredibly thankful for my amazing partner Lewis, to who I would not be who I am today, nor would I have been able to get this far without. I want to thank my parents for their love, support, and wisdom throughout my whole journey.

I would like to dedicate this thesis to my wonderful Nana; you are my everything.

Declaration

I, Ellie-May Redfern, declare that no portion of the work referred to in the thesis has been submitted in support of an application for another degree or qualification of this or any other university or other institute of learning.

Copyright Statement

i. The author of this thesis (including any appendices and/or schedules to this thesis) owns certain copyright or related rights in it (the "Copyright") and they have given the University of Manchester certain rights to use such Copyright, including for administrative purposes.

ii. Copies of this thesis, either in full or in extracts and whether in hard or electronic copy, may be made only in accordance with the Copyright, Designs and Patents Act 1988 (as amended) and regulations issued under it or, where appropriate, in accordance with licensing agreements which the University has from time to time. This page must form part of any such copies made.

iii. The ownership of certain Copyright, patents, designs, trademarks, and other intellectual property (the "Intellectual Property") and any reproductions of copyright works in the thesis, for example graphs and tables ("Reproductions"), which may be described in this thesis, may not be owned by the author and may be owned by third parties. Such Intellectual Property and Reproductions cannot and must not be made available for use without the prior written permission of the owner(s) of the relevant Intellectual Property and/or Reproductions.

iv. Further information on the conditions under which disclosure, publication and commercialisation of this thesis, the Copyright and any Intellectual Property and/or Reproductions described in it may take place is available in the University IP Policy (see http://documents.manchester.ac.uk/DocuInfo.aspx?DocID=2442 0), in any relevant Thesis restriction declarations deposited in the University Library, the University Library's regulations (see http://www.library.manchester.ac.uk/about/regulations/) and in the University's policy on Presentation of Theses.

Abbreviations	Definition
ASTER	Advanced Spaceborne Thermal Emission and Reflectance Radiometer
CAMS	Copernicus Atmospheric Monitoring Service
COMVOLC	Commission of Volcanology
CRB	Clouds as Reflecting Boundaries
CRED	Centre for Research and Epidemiology of Disasters
DOAS	Differential Optical Absorption Spectroscopy
ESA	European Space Agency
GFS	Global Forecasting System
GPS	Global Positioning Survey
HYSPLIT	Hybrid Single Particle Langrangian Integrated Trajectory
I-MORB	Indian Mid-Ocean Ridge Basalt
MCL	Main Crater Lake
MER	Mass Eruption Rate
MIROVA	Middle Infrared Observation of Volcanic Activity
MODIS	Moderate Resolution Imaging Spectroradiometer
NASA	National Aeronautics and Space Administration
NCEP	National Centre for Environmental Precition
NOAA	National Oceanic and Atmospheric Association
OCRA	Optical Cloud Recognition Algorithm
OMI	Ozone Monitoring Instrument
PHIVOLCS	Philippine Institute of Volcanology and Seismology
PHT	Philippine Standard Time (GMT + 8 hours)

PVMBG	Pusat Vulkanolog dun Mitgasi Bencana Geologi (Volcanology and Geological Hazards Mitigation Centre – Indonesia)
ROCINN	Retrieval of Cloud Information using Neutral Networks
SAR	Synthetic Aperture Data
SCD	SO2 Slant Column
Scontent	Sulphur Content
S5P	Sentinel-5 Precursor
TOA	Top of Atmosphere
TROPOMI	Tropospheric Monitoring Instrument
TVI	Taal Volcano Island
TVO	Taal Volcano Observatory
VAAC	Volcanic Ash Advisory Centre
VCD	Vertical Column Density
VEI	Volcanic Explosivity Index

Chapter 1. Motivation and questions

Volcanic plumes form from explosive eruptive events and are driven by exsolution of volatiles during magmatic ascent, resulting in the generation of large eruptive columns primarily composed of gas and fragmented silicate material (Durant et al., 2010; Grainger et al., 2013). The eruptive power and often long intervals of quiet dormancy of volcanoes makes them both difficult to study, and difficult to live nearby (Acocella, 2014; Dzurisin, 2003; Kelman and Mather, 2008). Existing and foreseeable advances in technology allow us to now consider a variety of questions critical to advancing our understanding of volcanic systems. Observational methods, such as surface deformation (Rosen et al., 1996; Lu et al., 2010; Mattioli et al., 2010; Hreinsdóttir et al., 2014; Wang et al., 2019; Meng et al., 2022), magma composition and volatiles (Haraguchi and Ishii, 2006; Ferlito et al., 2009), and thermal emissions (Ehara et al., 2005; Ganci et al., 2011, 2012) already allow limited volcanic eruption forecasting. Although earlier research has sought to understand each characteristic of a volcanic event using a combination of observational monitoring and satellite data, few have yet to combine an approach to obtain an understanding of the volcanic system as a whole for a wide region.

Since the introduction of scientific volcanic monitoring through the foundation of Osservatorio Vesuviano in 1845, today the World Organisation of Volcano Observatories has eighty members across the most volcanically active regions across the world (Sparks et al., 2012). Within these, the range and sophistication of the detection systems has increased dramatically, and advanced models of volcanic processes are helping to interpret monitoring data. In order to develop these models, research over the past 100 years has focused on the volcano as it erupts through sampling and observational methods (Pratt, 1911; Dailey, 1912; Gevers and Phil, 1940; Moore at al., 1966; Clark et al., 1977; Young et al. 1998) with modern advancements increasingly using satellite imagery (Iino et al., 2001; Wright et al., 2005; Wessels et al., 2021; Anantrasirichai et al., 2019; Schneider et al., 2020; Pandey et al., 2022). With an understanding of the volcanic processes during and after an eruption, research has been able to shift into understanding the precursory events to why a volcano erupts. Due to the nature of the volcano, it is difficult to predict and forecast an eruption as most volcanoes around the world are not monitored enough to find any significant changes in behaviour leading to an eruptive event (Marzocchi et al., 2012).

Satellite remote sensing has provided novel approaches to volcanic monitoring over the last few decades following the progress and introduction of each new satellite sent into orbit. Satellite monitoring can be divided into three categories: thermal monitoring, gas monitoring and deformation monitoring (which I do not focus on here). Satellite-based thermal monitoring can be further sub-divided into two groups: (a) automated detection of hotspots (using ASTER, MODIS-based automatic platforms such as MODVOLC (Jay et al., 2013; Wright, 2015) or MIROVA (Coppola et al., 2015, 2019, 2020; Massimetti et al., 2020) or SEVIRI-based automatic platforms such as HOTVOLC (Gouhier et al., 2016; 2020). And (b) quantification of thermal radiance using the MODIS equipment on board NASA's TERRA and AQUA satellites (Arellano-Baeza et al., 2007; Hernández et al., 2011). Volatile monitoring is achieved by using atmospheric gas quantifying instrumentation. NASA's AURA satellite, launched in 2004, is home to the Ozone Monitoring Instrument (OMI), a nadir-viewing wide-field-imaging spectrometer designed to provide high-resolution abundance monitoring of O_3, NO_2, and SO_2 (Riveria, 2011; Campion, 2014; Hayer et al., 2016; Liu et al., 2017). This paper will use OMI's upgraded replacement, the Tropospheric Monitoring Instrumentation (TROPOMI), launched in 2017, it provides a higher spatial resolution (3.5 x 5.5 km^2) and a higher signal-to-noise ratio-per-ground pixel (Theys et al., 2017, 2021, 2022; Queißer et al., 2019; Burton et al., 2021 Wang et al., 2022).

In this thesis I examine the SO_2 flux from degassing volcanoes across the Philippine and northernmost islands of Indonesia, with a particular focus on Taal volcano, in the period June 2018 – February 2022. Taal is the perfect candidate for this approach due to the limited gas monitoring as a result of its island-like structure within Taal Lake and the general challenge of monitoring gas emissions throughout an explosive event unless there is access to satellite data (Pallister and McNutt, 2015; Bignami et al., 2012). Quantifying the flux of volatiles from these volcanoes into the atmosphere is an important scientific aim because volcanoes are a key part of the global geochemical volatile cycle that provides an insight into the overall volcanic mechanism (Figure 1.1). Investigating each volcano's pattern and behaviour can allow an interpretation into each volcano's baseline degassing, allowing further insights into what can deemed as abnormal regarding activity. Understanding what is normal and what is abnormal regarding volcanic degassing is critical in understanding the personal driving mechanisms of a possible eruptions and further enhancing volcanic forecasting protocols. In addition, testing the capability of TROPOMI in volcanic monitoring throughout both degassing and eruptive events is crucial in developing innovative approaches to advancing

volcanic monitoring via satellite imagery. Knowing a volcano's pattern through its degassing and eruptive phases is also critical to understanding its individual precursory characteristics

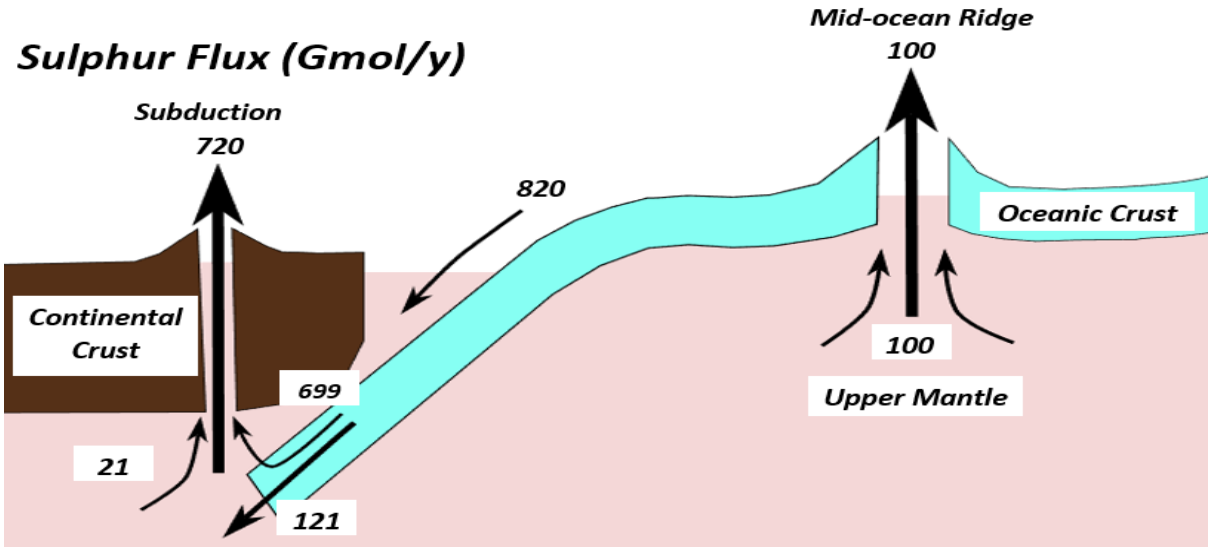

Figure 1.1. Schematic diagram depicting subduction-based volcanism and its role in the global sulphur biogeochemical cycle (adapted from Kagoshima et al., 2015).

before an eruption. According to The Centre of Research on the Epidemiology of Disasters (CRED) Disaster Events Database (EM-DAT 2013), during 1923 – 2023, volcanoes killed almost 40,000 people worldwide and affected almost 10 million. It is therefore vital to ensure their safety and survival that ongoing research actively seeks to advance monitoring techniques in fields which pose the most threat to human life (Paton et al., 2008).

The aim of this thesis is to use satellite data from TROPOMI, processed by the newly developed PlumeTraj toolkit (Burton et al., 2021; Esse et al., 2022), to quantify volcanic SO_2 emissions from the Philippine, Sangihe and Halmahera archipelagos. The key questions that will be addressed in this thesis include:

1. What were the gas emissions associated with the Taal eruption in January 2020, in terms of flux through time, total S release, injection altitude, and estimated magmatic $S_{content}$?
2. What was the nature of SO_2 emissions from Taal in the pre- and post-eruptive intervals, and how did this compare to other active volcanoes in the region?
3. Overall, what insights can we gain into volcanic processes from examining these results?

To achieve this aim, I have the following objectives:

1. To use PlumeTraj and TROPOMI data to calculate SO_2 flux and injection altitude time series.
2. To calculate the mass eruption rate and total magma $S_{content}$ throughout the January 2020 eruption.
3. To create an average monthly SO_2 mass (tonnes/day) profile for each volcano of interest in the study from June 2019 – February 2022

Chapter 2. Review of Literature

2.1. Geological Background of the Philippine Mobile Belt

The Philippine Island consists of two major tectonic blocks, the seismically-active Philippine Mobile Belt and the aseismic Palawan micro-continental block which both lie on the convergence of three major tectonic plate boundaries – Indo-Australian, Philippine Sea, and Sundaland (Figure 2.1b). The evolution of the Philippine archipelago can be accredited to the continued subduction, collisions and strike-slip faulting during the late Mesozoic and Cenozoic poly-phase activity (Queaño et al., 2015; Graciano et al., 2020).

The Eastern side of the Philippines, along the westward convergence of the Philippine Sea and Sundaland plates, accommodates the East Luzon Trough-Philippine Trench where subduction rates vary from 6 to 8 cm/yr (Aurelio, 2000). A product of this convergence, the Philippine fault zone is a left-lateral strike-slip system, which runs 1200 km through the whole arc from north to south. The western side of the Philippine island-arc system is bounded by the Manila-Negros-Cotabato trench system. The subduction occurring along the Philippine Trench produced the extensive volcanic arc along the eastern edge. The most prominent is the Bicol volcanic arc, which accommodates Mount Mayon (Figure 2.1a). As of 2018, the Philippine Institute of Volcanology and Seismology (PHIVOLCS) has listed 24 volcanoes as active within the Philippines, 21 of which have had historic eruptions. Some of the volcanoes in the Philippines rank as the most deadly and costly in the world: Auker et al. (2013) found that the Philippine and SE China regions averaged 47 fatalities per volcanic event, the second highest after the West Indies (201 fatalities).

Mayon volcano (13.26° N, 123.69° E) is located on Luzon Island in the Philippines, approximately 300 m southeast of Manila. Mayon is a basaltic andesitic, open-vent volcano

characterised by repetitive passive degassing from its summit at 2463 m above sea level (Ruth and Costa, 2021). Mayon follows a distinctive volcanic cycle of eruptive behaviour occurring approximately every 10 years for over a hundred years ranging from mid-size (<0.1 km^3) and mildly explosive to occasional phreatic eruptions (Ruth and Costa, 2021). Carn et al. (2017) using OMI found average SO_2 for Mayon during 2005-2015 were 453 t day^{-1}. Mayon sits along the Bicol Volcanic Arc, which forms from the westward subduction of the Philippine Sea Plate into the Philippine Trench (Figure 2.1a). The last known eruption was January 2018 which created a 1.3 km plume and 200-500 m lava fountains. SO_2 emissions reached 698 t day^{-1} on January 21, 2018 (PHIVOLCS, 2022). Mayon is a well-studied volcano with papers investigating volcanic deposits (Geronimo-Catane et al., 1991; Paguiran et al., 2009), mantle behaviour and source (Castillo and Newhall, 2004; McDermot et al., 2005), and plumbing system (Camacho et al., 2007; Vajda et al., 2012). During inter-eruptive periods, a persistent degassing is typically seen around the summit, between 400-600 tonnes of SO_2 per day (PHIVOLCS, 2019).

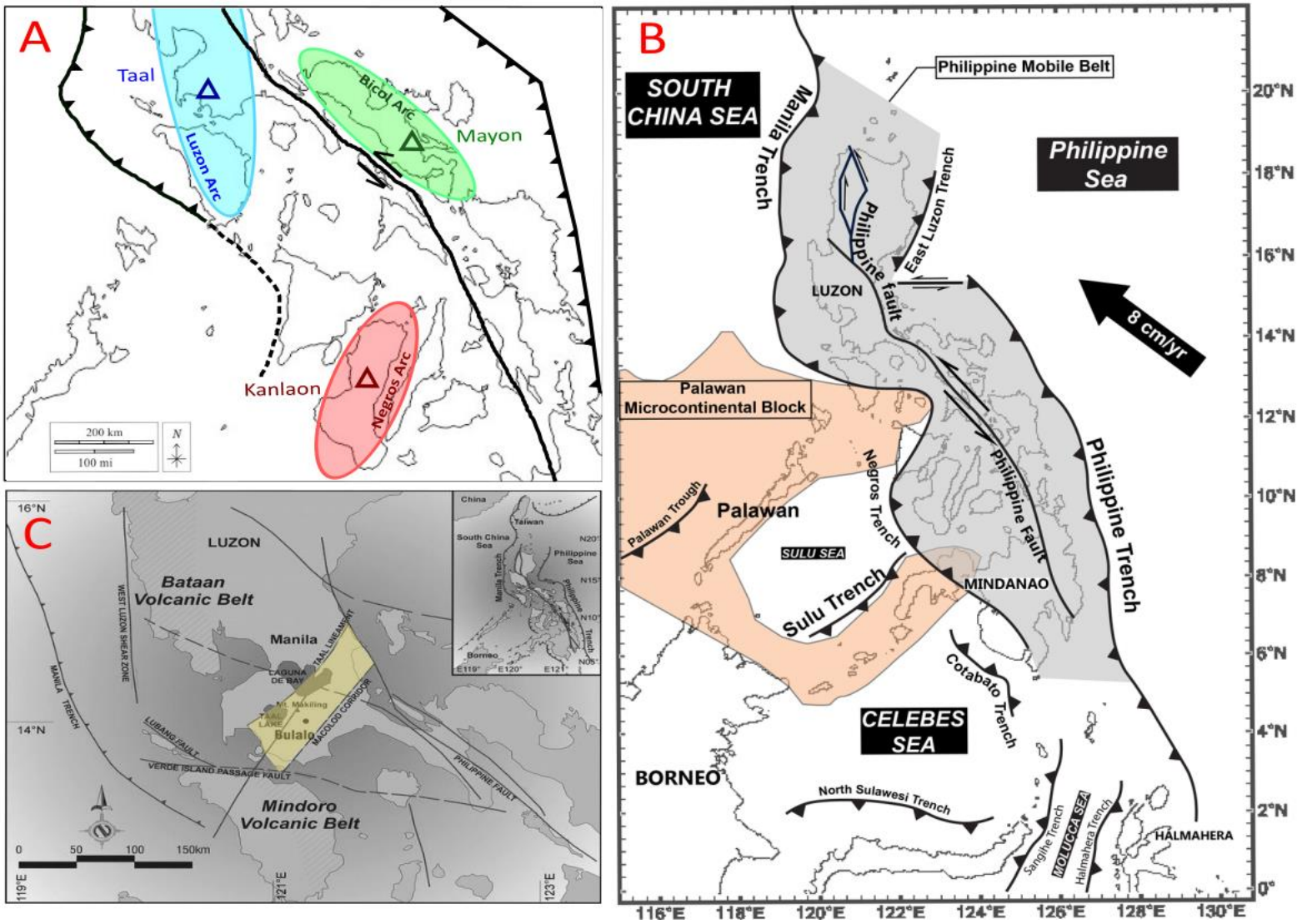

Figure 2.1. Map of the Philippines showing (A) regional position of Taal (blue), Mayon (green), and Kanlaon (red) in respect to the Luzon (blue), Bicol (green), and Negros (red) volcanic arcs, (B) position of Philippine Mobile Belt (grey) and Palawan Microcontinental Block (orange), and (C) position of Macolod Corridor relative to fault margins throughout Luzon (Adapted from Vicedo et al., 2008, ARTIGOS, 2023, Kumar and Singha, 2023).

Taal volcano (4.20° N, 20.39° E) is a 15 x 22 km prehistoric caldera within the Batangas Province on the south-western island of Luzon, Philippines. The volcano is one in a chain of active volcanoes that follow the eastward subduction of the South China Sea beneath the western region of the Philippine archipelago. The volcano is an approximately 311 m-high stratovolcano situated on Taal Lake, known to locals as Taal Volcano Island (TVI). The island lies on the intersection between the west Luzon calc-alkaline volcanic arc and the "Macolod Corridor", a NE-SW zone of extensive rifting through central Luzon which controls the Pleistocene to Holocene volcanism within the region (Lowry et al., 2000; Galgana et al., 2013, figure 2.1C). TVI is situated on a ridge that divides the Taal depression into two basins and is essentially a low-relief, post-caldera stratovolcano with numerous tuff rings and cones on its flanks (Delmelle et al., 1998). The caldera formed following at least four major, ignimbrite eruptions between 500 and 100 ka and is partially fault-controlled; a consequence of its location on a mosaic of regional fault structures (Lowry et al., 2001). Typically, volcanoes across Luzon are silicic in nature, most likely a result of the incorporation of terrigenous materials of the South China Sea through slab subduction (Miklius et al., 1991). The nature of volcanism across southwestern Luzon is varied, with basalts and andesites being found within the Quaternary volcanic deposits (Mikilius et al., 1991; Castillo and Newhall, 2003; Vogel et al., 2006).

Kanlaon volcano (10.24° N, 123.08° E) is located on Negros Island, Philippines, with a record of 30 historical events since 1866 ranging from phreatic to phreatomagmatic. It has developed a significant hydrothermal system within the volcanic edifice, which through time has evolved into two distinct systems independent of each other (Maximo et al., 2019). Volcanic activity stems from the Negros volcanic belt, which is a part of the Philippine microplate that extends ~260 km in N-S direction (Figure 2.1a). Carn et al., (2017) study using OMI found SO_2 emission averaged 70 t day^{-1} from 2005-2015. There are currently no scientific petrology or geophysics papers exploring Kanlaon's magma structure, plumbing, composition etc. however, a paper by Maximo et al. (2019) explores the geochemistry of the thermal waters from Kanlaon Volcano. They find that there are two hydrothermal systems working independently from each other: a mature and immature system. The mature system is characterised by neutral Na + K chloride (bicarbonate) whilst the immature is represented by acid-sulphate waters (Maximo et al., 2019). Regarding geochemical monitoring, it was concluded that the immature system (also referred as Hagdan Spring to locals) is influenced

by magmatic degassing and would be a prime candidate for future geochemical monitoring of Kanlaon.

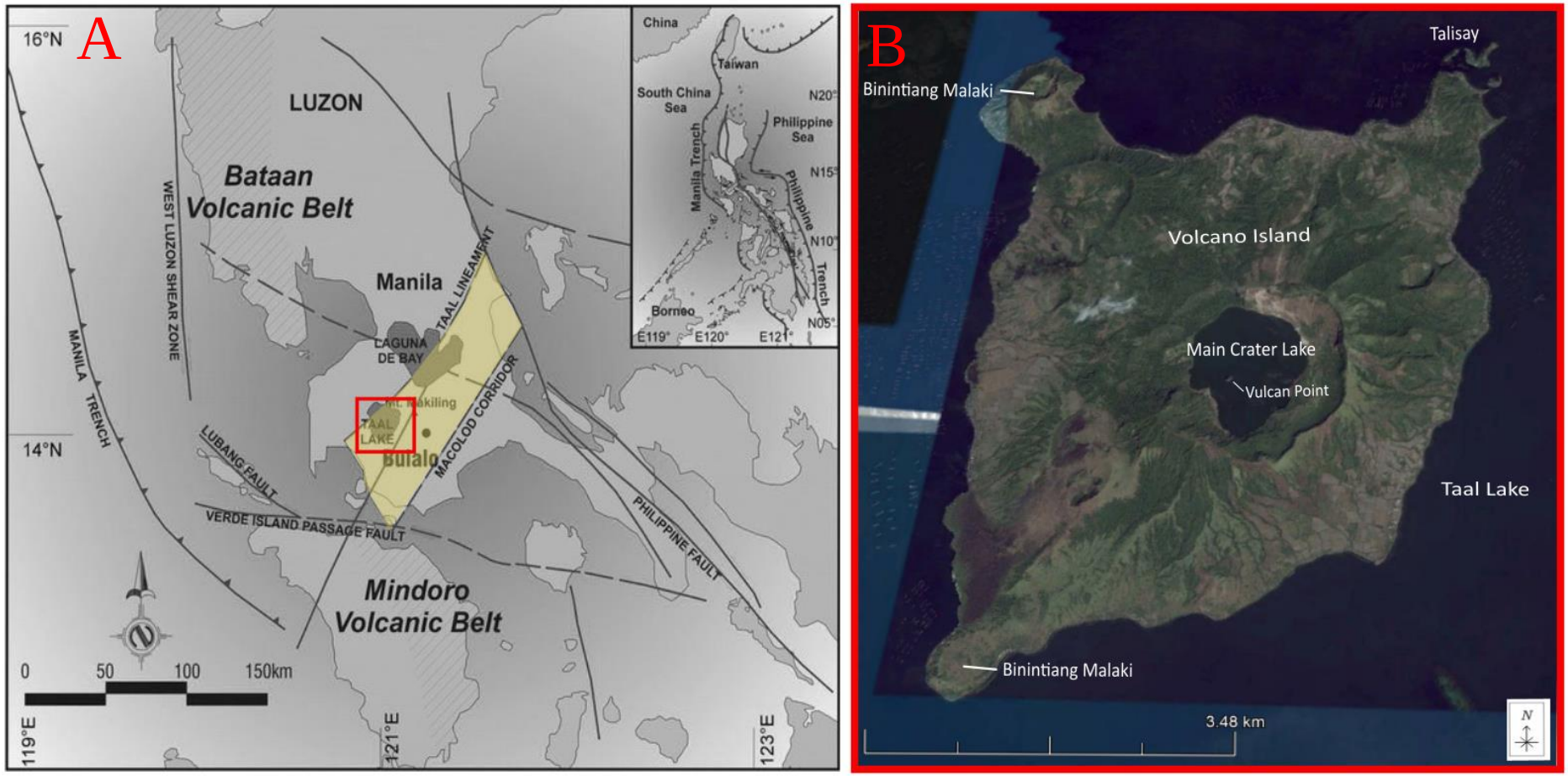

Figure 2.2. Map of the Philippines showing (A) position of Macolod Corridor relative to fault margins throughout Luzon and (B) labelled satellite imagery from 01/2015 of Taal Volcano Island using CNES Airbus (Adapted from Vicedo et al., 2008 and Google Earth, 2023).

2.2. Geological Background of the Sangihe and Halmahera Arcs

South-East Asia and areas of the western Pacific are located on the junction of three major tectonic plates (Eurasian plate, Indo-Australian plate, Pacific plate) which contribute to the complex mosaic of geology throughout the region including oceanic plates, island arcs, continental shelf, and crustal fragments (Villeneuve et al., 2002; Haberland et al., 2014). Excluding north-western parts of Java, the majority of the island seems to have been formed by two blocks: the SW Borneo block and the East Java-West Sulawesi block. Between the Sangihe island arc and Halmahera lies the Molucca Plate, which shows no surface expression but a collisional complex underneath the Molucca Sea between both arcs (Lallemand et al., 1998, figure 2.3, 2.4B). Due to the tectonic situation at the Molucca plate margin, two Benioff zones are found at either side of the sea creating the Sangihe island arc and the Halmahera Island arc complexes (Silver and Moore, 1978; Morrice et al., 1983, figure 2.3). The evolution of the islands across Indonesia have been long recognised that the region is a composite of allochthonous terranes that were accredited during the Palaeozoic to Cenozoic epochs (Audley-Charles and Hall, 1887; Metcalfe, 1988; 2013; Hall, 2012). Macpherson et al., (2003) magmatic geochemistry study across both the Sangihe and Halmahera arcs found that the mantle wedge differs between the two. Though both wedges composed of peridotite from the I-MORB, Halmahera lava contained distinctive peridotite with enriched I-MORB trace elements whilst Sangihe lava originated from the deformation of the upper North Sulawesi plate.

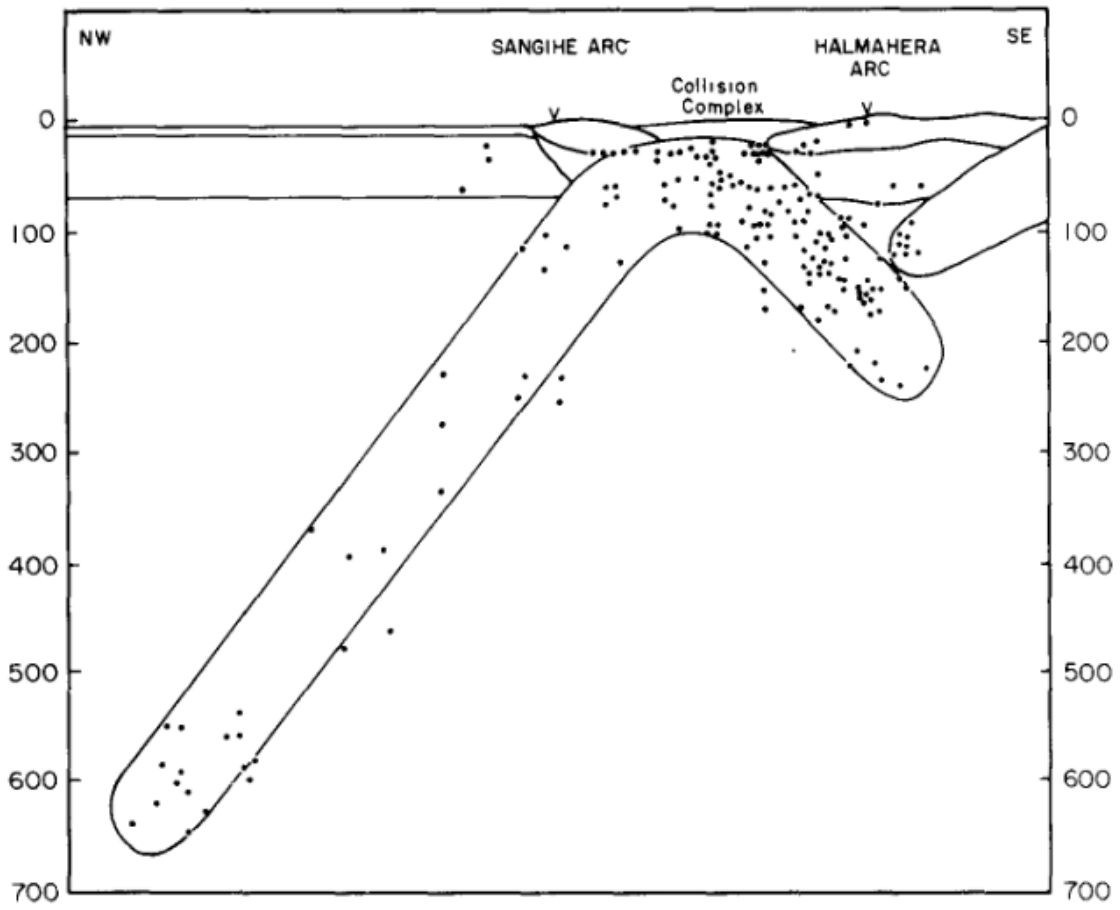

Figure 2.3. Lithospheric section across the Molucca Sea collision zone. Earthquake hypocentres are represented using dots (data obtained from Hatherton and Dickinson, 1969). V symbols mark active volcanic areas. No vertical exaggerations (From Silver and Moore, 1978).

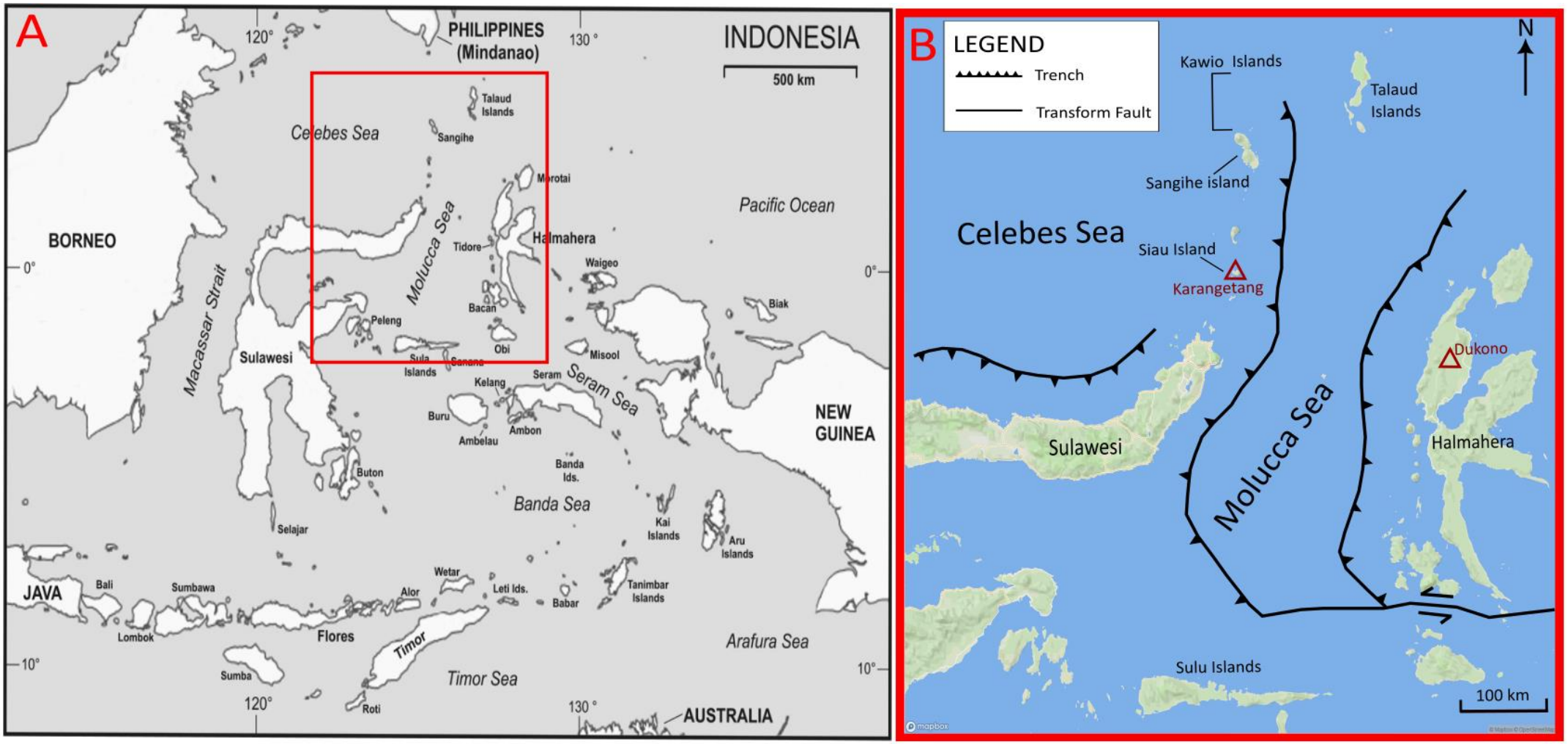

Figure 2.4. Map of NE Indonesia showing (A) geographical map of named islands and (B) regional position of Karangetang and Dukono relative to plate margins and corresponding island arcs (Adapted from Hennemann et al. 2015 and Theroux, 2023).

2.2.1. Sangihe Volcanic Arc, Sulawesi, Indonesia

The Sangihe island arc lies on the western side of the Molucca Sea region. Volcanism along the Sangihe arc is broken into the differentiated islands from north to south including Kawio Islands, Sangihe Islands, and northernmost Sulawesi. The Kawio groups contains nineteen small (<10 km^2) coral-fringed islands, twelve of which are composed of volcanic rocks (Morrice et al., 1983). The Sangihe islands contain four active volcanoes (Awu, Banua Wuhu, Api Siau, Ruang) that are relatively equally spaced (~50 km) apart down the island arc. Api Siau (125.41° N, 2.78° E) also known as Karangetang is a stratovolcano rising ~1770 m above sea level. The volcano has 5 distinct summit craters in a N-S line which have been responsible for 40 eruptions since 1675, making it one of the most active volcanoes within Indonesia (Morrice et al., 1983; Carn and Oppenheimer, 2000; Suwarsono et al., 2021). Volcanic activity has been frequent since 1675 and confined to the summit crater until the activity became increasingly explosive within the mid-1970s. Karangetang has been restless since Nov 2018 with periods of intense ash cloud formation, phreatomagmatic episodes (VEI = 2) and pyroclastic flows which are ongoing to date. Using the Ozone Monitoring Instrument (OMI), Karangetang averaged 313 t day^{-1} of SO_2 between 2005-2015 (Carn et al., 2017).

2.2.2. Halmahera Island Arc, Maluku, Indonesia

Halmahera is situated in eastern Indonesia adjacent to the southwest corner of the Philippine Sea plate, which stretches 300 km from north to south and 125 km east to west, with a distinct K shape (Hall, 1986, figure 2.5). The island exhibits the only example of arc-arc collision. The evolution of Halmahera can be traced back to its origins of Pleistocene arc volcanism where it was joined with the basement of east Mindanao, Philippines (Hall, 1986). Present-day volcanism is subjected to the subduction at the Halmahera Trench of the Molucca Sea plate (Figure 2.5). The island arc contains a chain of volcanic islands offshore of western Halmahera and volcanoes in the NW arm of the island (Hakim and Hall, 1991). The main island is home to five volcanoes including Dukono in the north and Ibu, Gamkonora, Uno, and Jailolo toward the south. Following the mountains along the south, other volcanoes on the islands include Gamalama on Ternate, Kie Matubu on Tidore, Kie Besi on Makian, and Buku Sibela on Bacan (Figure 2.5).

Dukono volcano (19.26° N, 155.14° W) is the northernmost active volcano on Halmahera Island, Indonesia (Figure 2.5). There are limited studies and information available due to the

remoteness of the island, but Dukono is one of the world's most active volcanoes, having been persistently active since 1933. Due to the varied power of eruptive activity, plume generation ranges from 0.3-2.4 km. Bani et al.'s (2017) analysis on Dukono's volcanic degassing using DOAS found that SO_2 emission fluctuated between 400-2000 t day^{-1}, with an average of 819 ± 235 t day^{-1}. Carn et al. (2017) found that using OMI, Dukono averaged 1726 t day^{-1} from 2005-2015. Assuming these figures are representative of the long-term volcanic degassing of Dukono, using Andres and Kasgoc (1998) volcanic sulphur emission inventory, Dukono's SO_2 output is comparable to Kilauea which resides in the top ten volcanoes for highest total SO_2 output. Bani et al. (2017) also found that Dukono's magma reservoir has changed from being a less differentiated source to a more evolved melt capable of sustaining explosive activity.

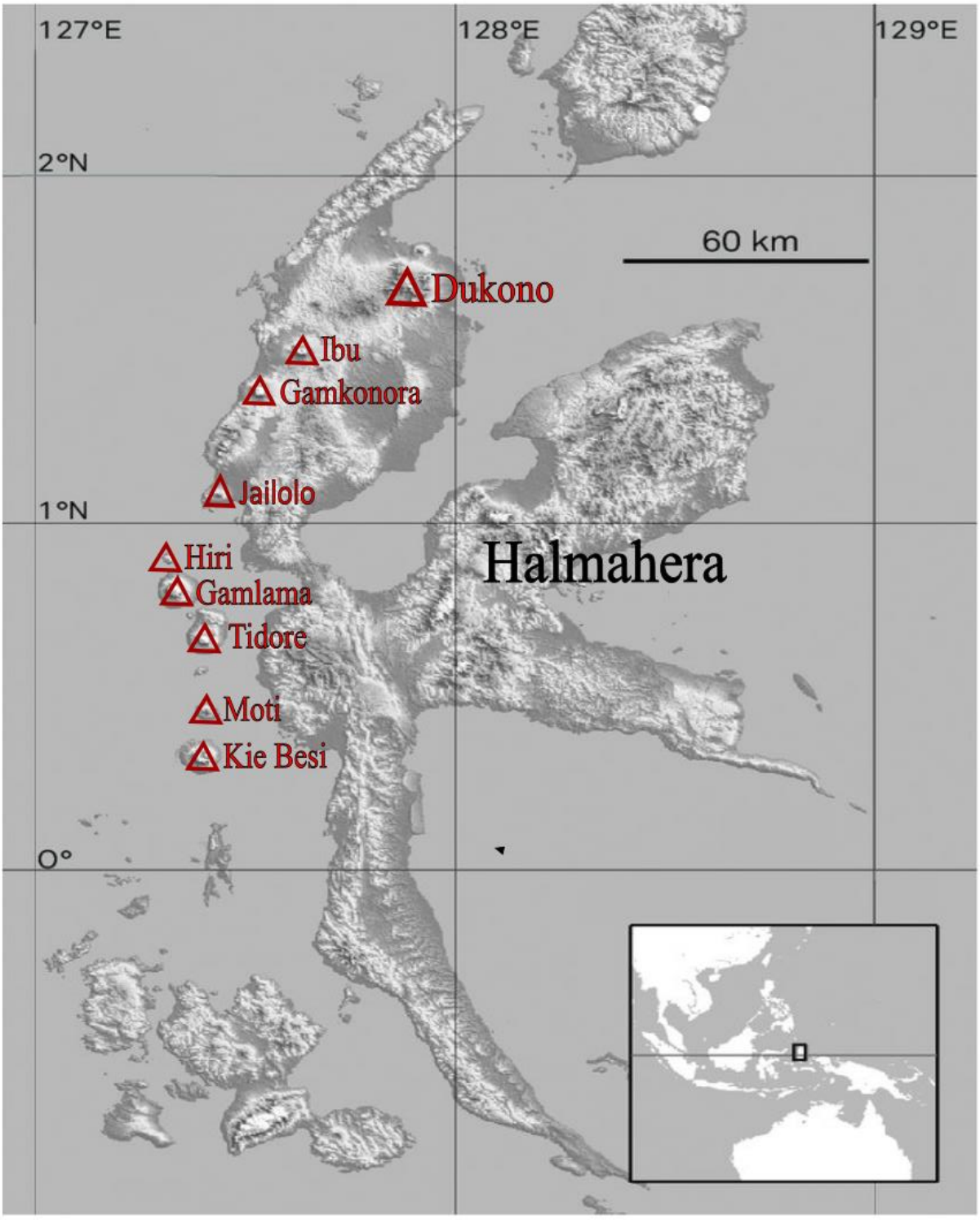

Figure 2.5. Map of Halmahera, Indonesia showing distribution of active volcanoes along the NW coast and western islands (adapted from Callmander et al., 2015).

2.3. Taal Volcano

2.3.1. Eruptive History and Deposits

Taal's frequent eruptions have given it the title of it being the smallest but most dangerous active volcano in the world, contributing thirty-four historical eruptions over the last two centuries (Delos-Reyes et al., 2018; Bato et al., 2021). The most notable historic eruptions include explosive events from 1716, 1749, 1754, 1911, and 1965 due to their intensity and impact within and around TVI. However, earliest reports date back to 1572 with eye-witness accounts claiming the occurrence of a phreatomagmatic eruption at the main crater.

Pakoksung et al. (2021) used a probabilistic tsunami hazard analysis approach to explore Taal's historic eruptive past. With a focus primarily on the 1716 eruption, the study found that the event was a subaqueous volcanic explosion located in the southern basin of the caldera, near the southern point of Taal Island. The decompressed gas within the surface resulted in the magma uplifting the water forcing a wave that inundated 17 m of land (Egorov, 2007). The 1749 eruption was characterised as being a violent phreatomagmatic eruption with a volcanic explosivity index equal to 4, which erupted towards the north of TVI, primarily affecting the northern shore villages. The only reference to the 1749 event is a Spanish illustrated record which details four volcanoes on Taal Lake erupting simultaneously and how a deadly gas engulfed the entire lake's population, killing an unspecified number of residents (National Historical Commission of the Philippines, 2023). Details of the 1754 eruption have been inferred from an eye-witness report of Father Buencochillo, an Augustinian priest who had witnessed the eruption from the town of Taal (Mojarro, 2020). His written account of the eruption matches descriptions of major plinian eruptions studied by scientists. The Philippine Institute of Volcanology and Seismology (PHIVOLCs) Director Renato Solidium Jr. said that the 1754 event is a classic plinian eruption defined as an "eruption of great violence characterised by voluminous explosive ejections of pumice and ash flows" (ABS-CBN, 2020). Solidium Jr. additionally referred to the likelihood that base surges and seiches generated a volcanic tsunami.

Entering the 20th Century, Taal's first major eruption occurred in 1911 with another phreatomagmatic to phreatic plinian eruption, ejecting a total of 80 million m^3. The eruption generated a pyroclastic density current which affected 15 km of land including the entire TVI and Talisay (Delos-Reyes et al., 2018; Saderra Maso, 1911). Masó (1911) describes the ejecta containing a combination of ash, mud, and some rocks forming a "huge column of

black smoke" lingering around the main crater. The tephra erupted formed ~ 20- 80 cm thick deposits that affected entire TVI and towns towards the west (Delos-Reyes et al., 2018). Another phreatomagmatic eruption occurring in 1965 generated a new cinder cone on the southwestern flank, causing a pyroclastic flow towards the south of the island. 40 million m^3 of tephra deposited itself around the main crater and the S-SW towns of Taal, leading to the accretion of 20-50 cm thick lapilli as far as 60 km (Delos-Reyes et al., 2018; Pakoksung, 2021). Moore et al. (1966) investigated the deposits from the 1965 eruption, determining the type and origin. It was found that the eruption generated two types of ejecta: (a) juvenile magmatic material from depth, and (b) shattered and pulverised old lava, ash, and lake sediments that filled the space of the crater prior to eruption (Moore et al., 1966).

The most recent explosive event was the January 12th 2020 phreatomagmatic eruption. The event has been classified as a VEI equal to 4 due to the large 15 km umbrella cloud plume, base surges, and heavy tephra deposits. A study focusing on documenting the 2020 eruption tephra deposits found that they consisted primarily of andesitic vitric fragments (83-90%) (Balangue-Tarriela et al., 2022). Other components of the fall deposits are lithic (7-11%) and crystal (less than 6%) grains (Balangue-Tarriela et al., 2022).

Although a 43-year dormancy period of Taal's eruptive activity progressed between the 1977 and 2020 eruptions, Taal hasn't been completely inactive. Taal's unpredictable nature has been associated with periods of seismic unrest and ground inflation. During 1991 to 1992, the caldera showed elevated seismicity, deformation, and increased crater lake temperatures that lasted from several days to months, but never escalated as far as an eruption (Global Volcanism Program, 1994). Bartel et al. (2003) revealed four stages of volcanogenic deformation from 1999 to 2000 with the largest displacement occurring between February-November 2000. This period of deformation was associated with ~120 mm of uplift of the centre of TVI relative to the northern caldera rim at average rates of up to 216 mm/yr. More recently, the 2010-2011 seismic crisis showed changes not only in caldera deformation but in the geochemistry of the Main Crater Lake (MCL). Hernández et al. (2017) found changes in chemical composition and an increase in dissolved CO_2 emission, particularly at the bottom of the lake. Their concluding remarks attributed this increase to a discharge of fluids rich in volcanic gases into the lake. These fluids were thought to have been a produced by degassing of a deep magma chamber whose interaction with the lake changed the overall geochemistry. Throughout the evolution of the crisis, changes in electric field, ground titling and uplift were also all recorded and associated with the interrelated stress changes, fluid/gas migration and

thermal activity within the deep hydrothermal system (Arpa et al., 2013; Hernández et al., 2017; Zlotnicky et al., 2018)

2.3.2. Deep Structure and Plumbing System

A multidisciplinary approach by Zlotnicky et al. (2017) using electromagnetic, geochemical, and thermal surveys found that the northern part of the volcano is the most active region, undergoing constant thermal transfers and degassing with volcanic activity taking place along the east-west trending fissure. Besana et al. (1995) concluded with their seismic topography survey of TVI that a low-velocity zone 18 km deep could be interpreted as the main magmatic source. Adding to that, Nishigami et al.'s (1994) previous research interpreted an additional shallow magma chamber at a 6 km depth in which fuels the ongoing volcanic activity seen today through its interaction with the hydrothermal reservoir directly above. A study investigating the hydrothermal reservoir under the TVI found that the body sits 500 m beneath an impermeable altered clay cap rock which holds >200°C water (Figure 2.6) (Yamaya et al., 2013). The shallow earthquakes seen around the island were accredited to the migration of water vapour through the fissures along the altered cap rock (Maeda et al., 2013).

2.3.3. Monitoring Taal

Scientific monitoring of Taal began in 1952 with the introduction of the first volcanological station in Brgy by the Commission on Volcanology (COMVOL) called the Alas-as station. The station was equipped with a three component, low sensitivity Akashi seismograph, a water tube tiltmeter, thermometers and short-wave radio transmitters (PHIVOLCS, 2022). As a consequent of the 1965 eruption, all of the monitoring equipment and large parts of the station were destroyed, leading to the introduction of the Pira-Piraso station on the northern shore, equipped with similar instrumentation. PHIVOLCS repeatedly replaced the equipment up until the construction of another observatory near Talisay called Buco Observatory. The observatory was equipped with a 3-component strong motion Inshimoto seismograph, a 3-component Hosoka seismograph, a short-wave radio transceiver and a speedboat. At the present day, the observatory is called the Taal Volcano Observatory (TVO) and is the main base of operations for monitoring the activity around the caldera. Regular monitoring systems

include water and gas geochemistry, ground deformation modelling (GPS and levelling) and seismology.

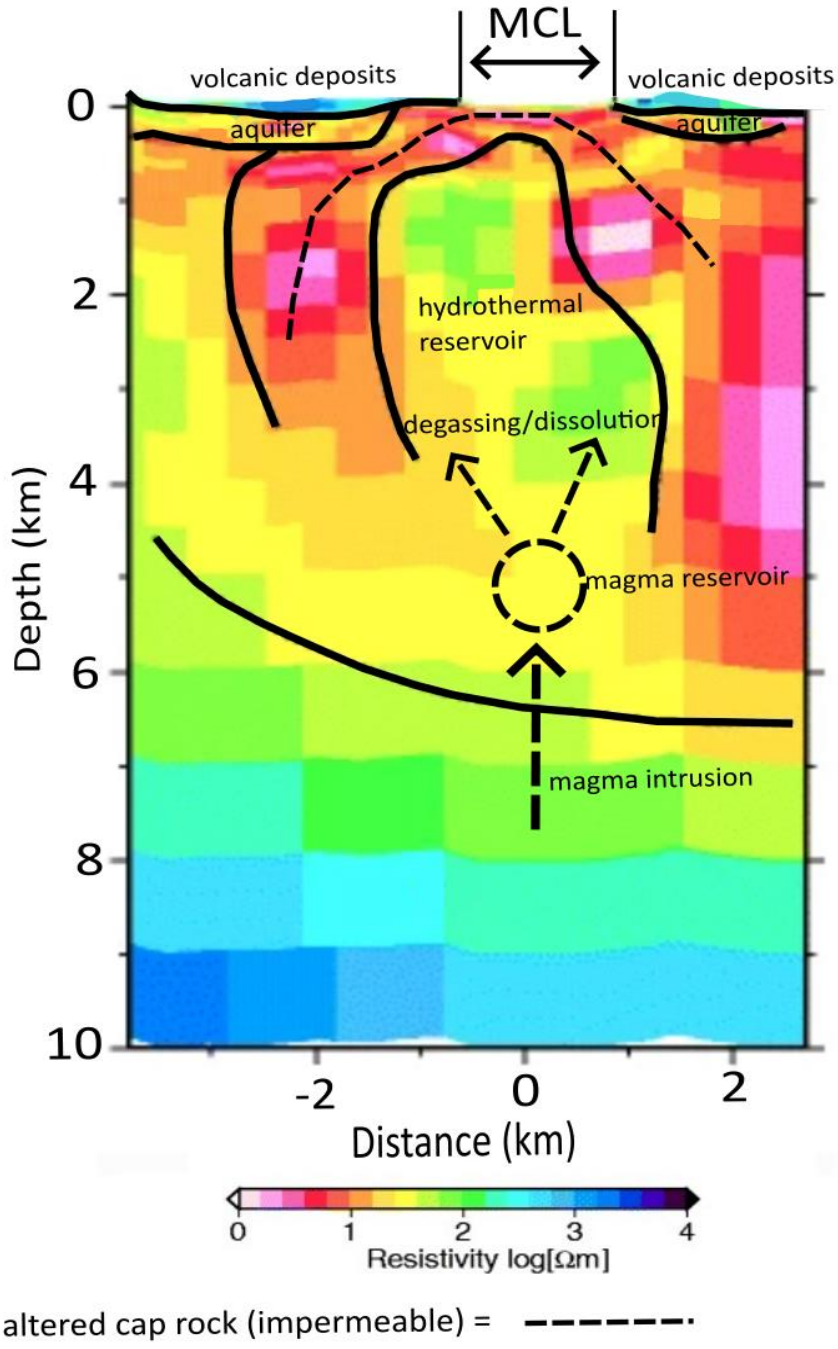

Figure 2.6. Two-dimensional inverted resistivity section of Main Crater Lake (MCL) (Adapted from Yamaya et al., 2013)

2.4. The January 2020 Eruption of Taal Volcano

2.4.1. Observational Reports

After 43 years of dormant activity, on 12th January 2020 Taal Volcano erupted initiating prolonged widespread interruption to the normal daily activities of the neighbouring populations. The plume height for the duration of the eruption varies between sources depending on the method of calculation. Plume heights from the use of infrasound found a mean height of 15 km and a maximum of 17 km (Perttu et al., 2020), whereas plume heights calculated from Sentinel-5P TROPOMI found SO_2 signals up to 20 km (Bachmeier, 2020) The first signal of an upcoming volcanic eruption can be traced back to more than 9 months prior to the 2020 event on 19 March 2019, where elevated seismicity was detected together with an increased inflation of CO_2 flux (Lagmay et al., 2021). On the 12th at 11:00 PHT, a series of seismic swarms occurred and two hours later a phreatic explosion took place 100 m deep within the Taal Volcano. PHIVOLCS alert system play a critical role at updating residents and authorities on the volcanic activity allowing them to prepare for evacuation protocols (Table 2.1). At 13:00 PHT, a phreatic eruption took place on the island raising the alert level from 1 to 2 for the surrounding Taal region, resulting in a precautionary evacuation of the immediate area conducted by PHIVOLCS. Upon immediate eruption, one death was attributed to rapid onset of the violent pyroclastic flow that formed immediately after the initial explosive event. His body was found amongst the ~1.5 m-thick pyroclastic deposits. At 15:00 PHT time, the eruption intensified producing a ~10 -km-high tephra column combined with volcanic lightning and intense ashfall. A further two hours later the alert level was raised from 2 to 4, which is accredited to a hazardous eruption being imminent. Consequently, a total evacuation of the Taal Volcano Island and areas within a 14 km radius from the main crater was implemented. At 18:49 PHT time, lava fountain occurred, and activity subsided before resuming as hydrovolcanic activity from the crater increased. On 26th January, the alert level was lowered from 4 to 3 due to the weakening state of magmatic eruptive episodes from the crater. February 14th saw the alert level decrease further from 3 to 2 and finally on March 19th the alert level declined to 1.

Table 2.1. Philippine Institute of Volcanology and Seismology (PHIVOLCS) volcano monitoring (alert levels) specifically for Taal volcano with monitoring criteria, interpretation, and recommendations for each alert level (1-5) (From PHIVOLCS, 2021).

Alert Level	Monitoring Criteria	Interpretation	Recommendation
0 Normal	**Background parameters:** Volcanic earthquakes typically <5/day; Main Crater Lake gas (diffuse CO2) emission within 1,000 tonnes/day, average water temperature <35ºC and acidity >pH2.5; General stationary or deflationary trends in ground deformation.	Quiescence: no major eruption in foreseeable future, but steam-driven and gas eruptions can occur without warning.	Permanent habitation on Taal Volcano Island (TVI) must not be allowed.
1 Low-Level Unrest	**Abnormal parameters**: Moderate level of seismic activity with some felt events; Main Crater Lake gas (diffuse CO2) emission >1,000 tonnes/day, slight increases in fumarole and/or Main Crater Lake temperatures and acidity; Slight and/or localized inflationary ground deformation changes in TVI.	Hydrothermal or tectonic activity beneath the volcano may be occurring; steam-driven, gas or hydrothermal explosions can occur without warning.	Entry into the TVI Main Crater, the Daang Kastila fissure area and the Mt. Tabaro eruption site must not be allowed
2 Increasing Unrest	**Increasing changes in parameters**: Elevated level of seismic activity with some felt events in TVI and Taal Caldera (TC); Occurrence of earthquake swarms and low-frequency events; Sustained increases in inflationary ground deformation including ground tilt in TVI; Slight positive microgravity changes in TVI and TC; Increasing fumarole temperature and acidity and upwelling in the Main Crater Lake; Significant increases in CO2 emission, instrumental detection of airborne SO2 >500 tonnes/day.	Shallow hydrothermal unrest and/or deep-seated magmatic intrusion may be occurring, bringing higher chances of steam-driven, gas or hydrothermal explosions.	Entry into TVI must not be allowed. Communities in pre-defined areas of the highest hazard must be ready for possible evacuation.
3 Intensified Unrest/ Magmatic Unrest	**Intensifying changes in parameters**: Sudden increase or decline in seismic activity; Perceptible earthquakes, occurrence of swarms of volcano-tectonic and/or hybrid earthquakes; Elevating SO2 flux; Significant changes in Main Crater Lake temperature and/or acidity; Accelerating increase in ground inflation, rapid increase in ground tilt in TVI; Precursory phreatic or weak phreatomagmatic eruptions commence.	Magmatic or explosive phreatomagmatic eruption is imminent; precursory eruptive activity may be taking place and generating ashfall, ballistics and/or short lava flows.	TVI, Taal Lake and pre-defined lakeshore communities of Batangas facing the active vent must be evacuated.
4 Hazardous Eruption Imminent	**Accelerating changes or abrupt decline in parameters**: Rapidly intensifying volcanic earthquakes, continuous volcanic tremor, frequent felt earthquakes; Profuse degassing or ash explosions along existing or new vents and fissures; Elevated and/or sudden drop in SO2 flux; Accelerating increase or reversal of ground deformation patterns and ground fissuring; Explosive eruption or lava effusion with or without volcanic lightning commence.	Strong phreatomagmatic or magmatic eruption is taking place, which may or may not lead to violently explosive eruption. Widespread ashfall and ballistics, lava flows and minor pyroclastic density currents (PDCs) on TVI may be generated.	Communities in pre-determined worst-case or scenario-based volcanic hazards zones must be evacuated.
5 Highly Hazardous Eruption Imminent	**Violently explosive magmatic eruption ongoing**: Continuous intense seismic activity, including explosion-type volcanic earthquakes and strong felt events; Sustained tall eruption column with expansive umbrella cloud accompanied by loud booming sounds and volcanic lightning; Generation of PDCs/base surges and volcanic tsunami that transport across Taal Lake and lakeshore towns; Ground fissuring and large-particle tephra fall impacting lakeside communities and ashfall impacting farther areas.	Plinian/ Subplinian/ Violent phreatomagmatic eruption is taking place. Extreme life-threatening hazards of base surges/PDCs, volcanic tsunami, thick tephra fall/ashfall, fissuring, lahars, and landslides.	Additional areas for evacuation should be considered based on prevailing conditions.

Time-series imagery and video analysis of the 2020 eruption found that the activity had generated a vertical volcanic eruption column consisting of a gas thrust (jet) region, a convective region, and an umbrella region (Lagmay et al., 2021) (Figure 2.7). Ballistic volcanic bombs and laterally moving flows (basal clouds) were observed from the gas thrust region, which rose ~130 m above the main crater rim. The observed basal clouds travelled at 50-60 ms^{-1} outwards from the initial gas thrust region around the base of the main crater. Within the convective phase, air obtained from around the column continued to expand the plume reducing its overall density, resulting in the amalgamated hot gas and pyroclasts to rise, forming a grey-coloured column of thickened clouds. By 16:00 PHT, a north-driven umbrella cloud was well-established, which by approximately 20:00 PHT time reached a height of 17-21 km, with an E-W diameter of ~100 km (Lagmay et al., 2021). The diameter and height of the umbrella cloud achieved is consistent with eruptive events characterised by mass discharge rates in the order of 10^8 kg s^{-1} equivalent to a Volcanic Explosivity Index (VEI) equal to 4 (Constantinescu et al., 2021, Table 2.2). During the peak of the eruption, all the monitoring instruments installed on Taal were damaged or completely destroyed, temporarily stopping their operation (Sabillo, 2020). Consequently, PHIVOLCS were forced to use low-latency synthetic aperture radar (SAR) data which provided the only insight to the ongoing state of the volcano, allowing the forecast of possible eruption scenarios.

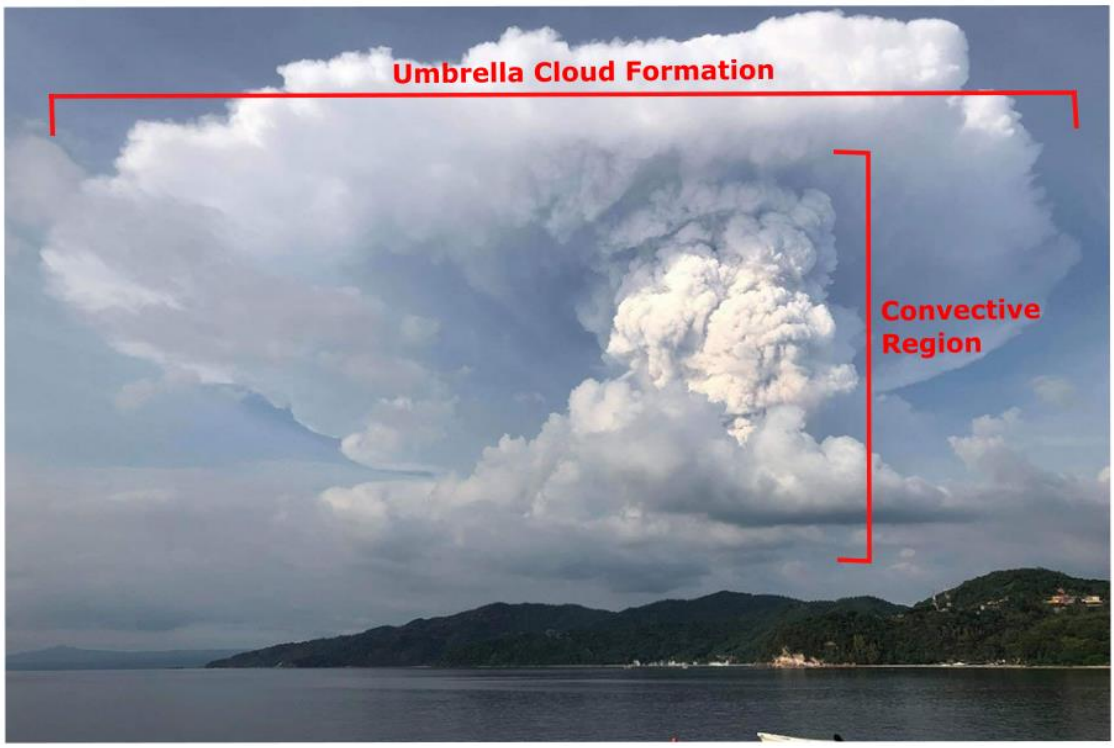

Figure 2.7. Image captured on 12 January 2020 during peak eruption showing vertical convective region and the formation of the umbrella cloud. Image credit: Danny Ocampo.

Table 2.2. Volcanic Explosivity Index (VEI) updated with umbrella cloud radius as an additional classification criterion (From Constantinescu et al., 2021).

Criteria |VEI	0	1	2	3	4	5
Volume of ejecta (m^3)	$<10^4$	$<10^6$	$<10^7$	$<10^8$	$<10^9$	$<10^{10}$
Column height (km)	<0-1	0 - 1	1 - 5	3 - 15	10 - 25	>25
Umbrella cloud radius (km)	-	$<10^b$	$<10^b$	<10	10 - 100	100 - 200

[b]Plumes of translent eruptions will also develop gravitationally spreading clouds at the neutral buoyancy level, although of limited radil due to mass discharge rates

2.4.2. Eruption Dynamics

There were no indicators of any magmatic changes seen within the months leading to January 2020 through observational reports other than slight ongoing inflation within the edifice since March 2019 (PHIVOLCS, 2019). However, within a normal volcanic lake system, it is typical to see changes in lake geochemistry regarding acidity and concentration of elements/compounds with increased activity (Varekamp, 2015; Delmelle et al., 2015). However, at Taal, groundwater beneath the lake drowns the magmatic heat and gas flow to the surface, causing Taal lake to be mildly acidic opposed to the expected highly. Therefore, the volcano can be interpreted as quiescent or dormant, even if there are ongoing intense alterations to the magmatic system (Delmelle et al., 2015). PHIVOLCS suggest that the eruption was a consequence of an injection of fresh magma into Taal's volcanic system. The eruption was later categorised as a phreatic explosion between the heat of the injected magma and abundance of water producing a steam driven explosion (Figure 2.8).

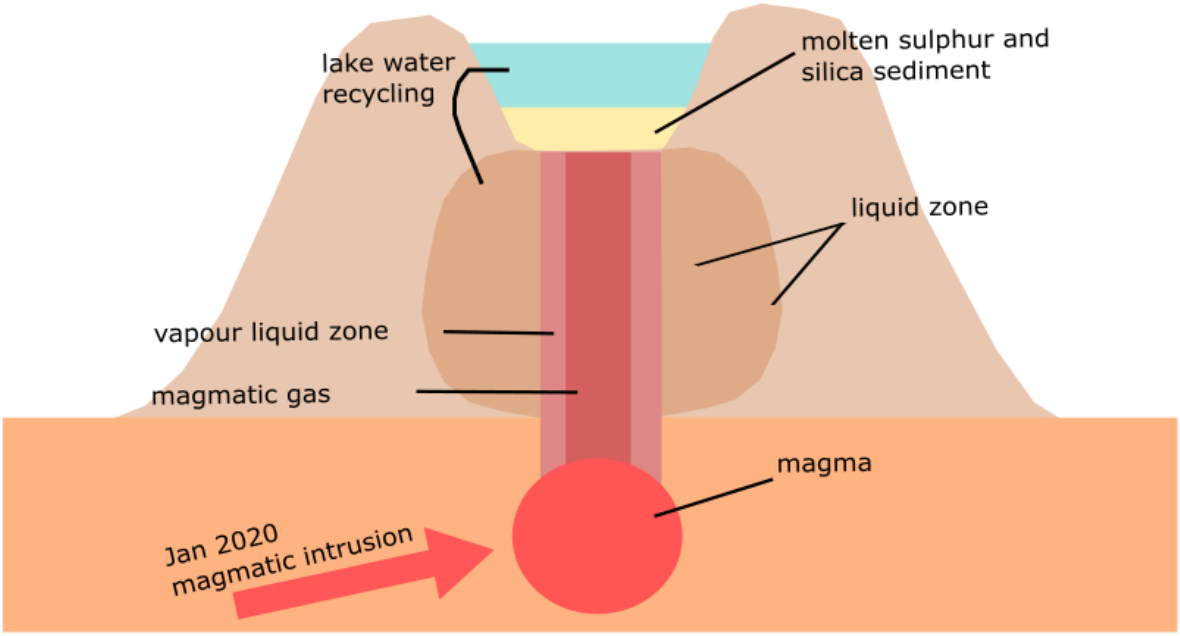

Figure 2.8. Cartoon diagram illustrating the association between an acidic crater lake, and a hydrothermal system powered by a shallow magmatic intrusion. Diagram also illustrated the proposed magmatic injection into the original intrusion causing an intensification of the magma pressure and heat (Adapted from Delmelle et al., 2015).

Chapter 3. Measurements of SO_2 degassing from space

Having an accurate repository of the current spatial and temporal distribution of volcanic gas emissions globally is critical for numerous applications, ranging from rudimentary volcanic monitoring to assessment of the impacts of volcanic degassing on the wider Earth system (Ebmeier et al., 2018; Furtney et al., 2018; Marchese et al., 2010). Sulphur species, primarily sulphur dioxide (SO_2), are fundamental in monitoring due to the ease of quantitative measurement from ground- and satellite-based remote sensing (Carn et al., 2017). They also provide a key role in the Earth's volcanic geochemical cycle and the processes responsible for volcanic impacts on the environment, atmospheric chemistry, and climate (Carn et al., 2017). Sulphur (SO_2) is introduced into the atmosphere and hydrosphere through the discharge of gas from volcanic and hydrothermal activity (Lagmay et al., 2021). The global geochemical flux and mass of SO_2 from sub-aerial volcano arcs can be determined by using UV spectroscopy (Dwyer et al., 2003), and satellite remote sensing (Corradini et al., 2021). Over recent years, a shift in focus onto creating a global SO_2 repository for active volcanoes worldwide has been seen with the introduction of Carn et al.'s (2017) decade of global volcanic SO_2 emissions measured using the Ozone Monitoring Instrument (OMI) on NASA's Aura satellite from 2005 – 2015. The NASA repository also contains global SO_2 emissions that record near-real time images using the Suomi NPP satellite which provides well calibrated measurements from two nadir sensors and an additional sensor looking at the atmospheric limb (https://ozoneaq.gsfc.nasa.gov/data/omi/#). Though these images are insightful in visualising SO_2 concentrations within the Earth's atmosphere, they do not provide a quantification of the total measured SO_2 or any insight into the fluxes of the Earth's volcanoes.

3.1. Review of TROPOMI SO_2 papers

Active volcanoes around the world emit SO_2 during both quiescent, background activity, and violent, short-lived eruptions. Measurement of volcanic gas fluxes are essential in understanding eruption forecasting and can be used to infer the quantity, composition, and storage conditions of magma within the Earth (Carn et al. 2021). The detection of lower altitude volcanic plumes within the troposphere emitted by passively degassing volcanoes are of potential value to volcanic monitoring as understanding the passive state is crucial in understanding what a quiescence period looks like allowing access to understand abnormal activity leading to an explosive event. Whilst ground monitoring techniques provide

relatively accurate insight into passive degassing of a volcano, the measurements are easily influenced by the presence of ash plumes causing discrepancies with the data acquired. Explosive activity in the form of pyroclastic currents, volcanic ejecta and heavy ash fall damages and destroys the monitoring network, while any means of direct manual measurements are too dangerous to perform. Satellite SO_2 instrumentation can use two types of sensors: ultraviolet (UV) and infrared (IR). Satellite monitoring provides frequent daily coverage of temporal and spatial variances of any given area across the world aiding in filling potential monitoring gaps from ground-based monitoring (Furtney et al., 2018). Access to satellite observations is critical in monitoring remote or inaccessible volcanoes such as Karangetang and Dukono. In addition, these volcanoes are highly active with frequent explosive eruptions that would decimate ground-based instrumentation within their vicinities proving that satellite instrumentation is possibly the only way in which these volcanoes can be monitored (Bani et al., 2018; Santoso et al., 2022).

Since the launch of the Sentinel-5P satellite in October 2017, the global volcanological community have exploited and published numerous papers discussing the advantages to this new instrumentation for volcanic monitoring (Pardini et al., 2017, 2018, 2019; Theys et al., 2017; Kleipool et al., 2018; Hedelt et al., 2019; Queißer et al., 2019; Ialongo et al., 2020; Ludewig et al., 2020; Burton et al., 2021; Cofano et al., 2021; Pandey et al., 2022; Wang et al., 2022). A large collection of papers investigate specific eruptions that have occurred after the launch to quantify the volcanic volatiles using TROPOMI and explore how these datasets can be manipulated and analysed. Inness et al. (2021) investigated the use of the Copernicus Atmospheric Monitoring Service (CAMS) in conjunction with the measurements obtained from TROPOMI which allowed the system to forecast the overall location of the Raikoke SO_2 plume up to 5 days in advance for about 20 days after the initial eruption as well as the retrieved SO_2 data. Other papers looked into solely using the retrieved vertical column density (VCD) of retrieved SO_2 to produce a time flux series for both short and long-term degassing and explosive events (Queißer et al., 2019; Burton et al., 2021; Pandey, 2022). However, published papers have criticised the instrumentation deeming it to produce an overestimation of SO_2, especially in regions where there are clusters of volcanoes (Cofano et al., 2021) or an underestimation of SO_2 when compared to ground-based monitoring of the same region of interest (Wang et al., 2022). Due to the nature of TROPOMI and its relatively new introduction into the volcanological community, there is always room for improvement

and a change in research interest is now aimed at improving the retrieval algorithms thus ensuring a reliable analysis and interpretation (Wang et al., 2022).

PlumeTraj is a software toolkit designed to reconstruct volcanic SO_2 fluxes using SO_2 data from TROPOMI onboard the European Space Agency (ESA) Sentinel-5P Precursor (S5P) satellite and NOAA's HYSPLIT software with three-dimensional (3D) wind fields from the National Oceanic Atmospheric Association (NOAA) National Centres for Environmental Prediction (NCEP) Global Forecast System (GFS) (Pardini et al., 2017, 2018, 2019). PlumeTraj takes the static image of SO_2 distribution measured by TROPOMI and reconstructs the time- and altitude-resolved fluxes using back-trajectory analysis (Pardini et al., 2018, 2019; Queißer et al., 2019). Altitude is a key variable in the creation of SO_2 vertical column densities (VCD). However, without the introduction of time as a variable, there can be no reconstruction of SO_2 flux for the duration of an eruptive event. The introduction of the back-trajectory approach overcomes this limitation and therefore, flux retrievals may be achieved with reasonable confidence (Queißer et al., 2019). Back-trajectory analysis is a commonly used approach within the study of transport paths of ash, aerosols, and gases dispersed into the atmosphere from both natural and anthropogenic sources (Cape et al., 2000; Freiman and Piketh, 2003; Song et al., 2008; Zhu et al., 2011).

Chapter 4. Methodology

4.1. TROPOMI

TROPOMI is a passive-sensing hyperspectral imager located on the ESA-S5P, launched into orbit on 13th October 2017. The instrument has the capability to measure reflected sunlight in the ultraviolet, visible, near-infrared, and shortwave infrared spectral ranges. The spectra measured are processed and used to obtain the total column of trace gases, including sulphur dioxide (SO_2) (Queißer et al., 2019). SP5 is a sun-synchronous, low-Earth orbit (824 km) satellite, which has an almost full-earth-surface coverage on a daily basis.

The TROPOMI data is received in the netCDF-4 format (.nc) from offline Level 2 (L2) SO_2 geophysical data products, which is freely obtained via the ESA-Copernicus Sentinel-5P Pre-Operation Data-Hub. The SO_2 slant columns (SCD) are obtained by using Differential Optical Absorption Spectroscopy (DOAS) using ground-reflected solar UV light as the primary source. In order to obtain a vertical column density (VCD), the SCD must be divided by a pre-determined air mass factor (AMF). However, in order to achieve an accurate VCD, the

SO_2 altitude needs to be known at the time of the eruption. To address this issue, three VCDs are used within this study which include 1km interval plots at: 0-1 km above ground level, 6.5-7.5 km above sea level, and 14.5-15.5 km above sea level. In this study, these three VCD are referred to as 1 km, 7 km, and 15 km.

An implication of this approach is the presence of difficult observation conditions (i.e., optically thick ash plumes) and chemical interfering species (i.e. clouds, aerosols), the representation of vertical profiles (gas, temperature, pressure), and uncertainties on data from external sources (e.g. surface reflectance) (Theys et al., 2022, 2021, 2017). Corradini et al. (2009) found a significant SO_2 overestimation during and after a volcanic eruption where ash and SO_2 had been emitted simultaneously. The ash particles (from 1 to 10 μm) within the plume tend to reduce the Top of Atmosphere (TOA) radiance in most satellites spectral range, including the channels used for the SO_2 retrieval (Corradini et al., 2009). TROPOMI measures in three different spectral ranges including ultraviolet and visible (0.27-0.5 μm), near-infrared (0.68-0.78 μm), and shortwave infrared (2.31-2.39 μm), therefore interpretation of the results within the study must be taken with care.

4.2. PlumeTraj Method

PlumeTraj is an advancement on the approach demonstrated by Pardini et al. (2017). This approach uses a combination of forward and backward trajectories by adopting a two-step procedure in order to improve the quality of plume height and SO_2 flux. In order to reconstruct a SO_2 flux time series, a series of values are needed which include known plume altitude at the specific time and location by satellite and the accurate corresponding VCD, injection time and altitude from the volcano. PlumeTraj is a back trajectory approach and multiple steps are required in order to be able to present the data within this study which will be outlined.

Raw SO_2 data from TROPOMI is refined using the Burton et al. (2021) technique used for the White Island/Whakaari 2019 eruption. Raw SO_2 data from TROPOMI is first filtered for noise by removing high-noise SO_2 pixels (those with SO_2 less than three times reported SO_2 error). A secondary filter is required to remove pixels that are not adjacent to more than two pixels that have passed the first filter threshold. This process will allow a total fixation on the pixels that are associated to the plume by removing lone pixels that may not be associated with the eruption or are errors. However, a downside of this approach is that there is a chance of an underestimation of the SO_2, but the process allows total removal of potential noise,

improving the overall quality (Burton et al., 2021). The pixels are then ready for the back-trajectory analysis using a combination of Hybrid Single-Particle Langrangian Integrated Trajectory model (HYSPLIT) and three-dimensional (3D) wind fields from the National Oceanic and Atmospheric Association (NOAA) National Centres for Environmental Production (NCEP) Global Forecasting System (GFS) to determine the age and height of each pixel in the image and correct the height-sensitive vertical column density of SO_2 in each pixel. HYSPLIT models stimulate the dispersion and trajectory of substances transported and dispersed through the atmosphere, across local to global scales. HYSPLIT can be integrated with PlumeTraj to refine the data output and consequently the projected images of an event. The trajectories are mostly calculated 24 hours back in time.

4.2.1. Averaging Approach

An averaged approach was used in order to gain insight into volcanic SO_2 emissions across the Philippines and the northern-most islands of Indonesia. A series of images (Figure 4.1) with corresponding data files were collected using this approach allowing a visualisation of the daily SO_2 emissions per month (t day^{-1}) from each volcano within the region. To achieve this, every overpass each month was taken and stacked together producing a total monthly VCDs. The data was then compressed down into a single .nc file to produce a vertical column density for 1 km, 7 km, and 15 km. As my aim was to investigate the regional degassing, 1 km vertical column densities were used across each volcano of interest which may cause an underestimation of larger explosive events.

To convert the VCDs into daily SO_2 emission per month (t day^{-1}), steps were taken using the pixels surrounding each volcano. First of all, a boundary had to be established to work out the total area of the pixels which would be used in finding the SO_2 emission using equation (c) below:

$$daily\ SO_2\ emission\ per\ month\ (g\ day^{-1}) = \left(\frac{VCD\ \left(\frac{mol}{m^2}\right) \times Area\ (m^2)}{6.022 \times 10^{23}\ mol^{-1}} \right) \times 64.066\ \left(\frac{g}{mol}\right)$$

The boxes were tailored to each volcano whilst attempting to encompass as much as the total plume which originated from each volcano (Appendix A). The size of the box was determined by running each individual month and identifying the outermost pixels that belonged to each volcano. The furthest pixels away were used to draw the edges of the box

ensuring as much as the SO_2 pixels were encompassed. Consequently, each volcano has a different sized box as a result of the varying activity from explosive to dormant. Though this is not the most accurate approach, it will give a generalised idea to the emission rate and SO_2 mass emitted from each volcano. Once each box is established, a tailored code was used to calculate the total pixel area using the latitude and longitude. The code was then programmed to produce a .csv file output for each volcano where the units were converted from grams to tonnes for total SO_2 mass by multiplying by a factor of 10^6. Eruptions that exceeded <2000 t day^{-1} were taken out of the final analysis in order for a better comparative analysis for general degassing patterns also allowing a consistent y-axis across each volcano.

4.2.2. Cloud Fraction

Cloud fraction is an important variable due to the strong impact clouds have on satellite measurements of tropospheric trace gases in the ultraviolet, visible, and near-infrared spectral ranges from space (Compernolle et al., 2021; Latsch et al., 2022). The interplay of sunlight with clouds imposes major challenges for satellite remote sensing with the top three complications being (a) the albedo effect, (b) the "shielding" effect, by which the trace gases are hidden underneath the clouds themselves, and (c) the increase in absorption within the cloud (Liu et al., 2004; Kokhanovsky and Rozanov, 2008; Wagner et al., 2008). Clouds can exacerbate the process of chemical and physical alterations of SO_2 converting the volcanic gas into sulphates (SO_4^{2-}) through oxidation (Ali-Khodja and Kebabi, 1998; Zhang et al., 2018). The operational TROPOMI cloud product uses Optical Cloud Recognition Algorithm (OCRA) and Retrieval Of Cloud information using Neutral Networks (ROCINN) CRB (Clouds-as-Reflecting-Boundaries) (Loyola et al., 2018). Cloud data was received using OCRA/ROCINN CRB as a combined .nc file with other TROPOMI products. The .nc file was converted to a .csv file using Panoply. The data within the cloud .csv file showed the cloud fraction for each pixel within the total area. A scene-wide average was taken across all the pixels available within the area, producing the average cloud fraction for 12/01/20 and 13/01/20 (Appendix B).

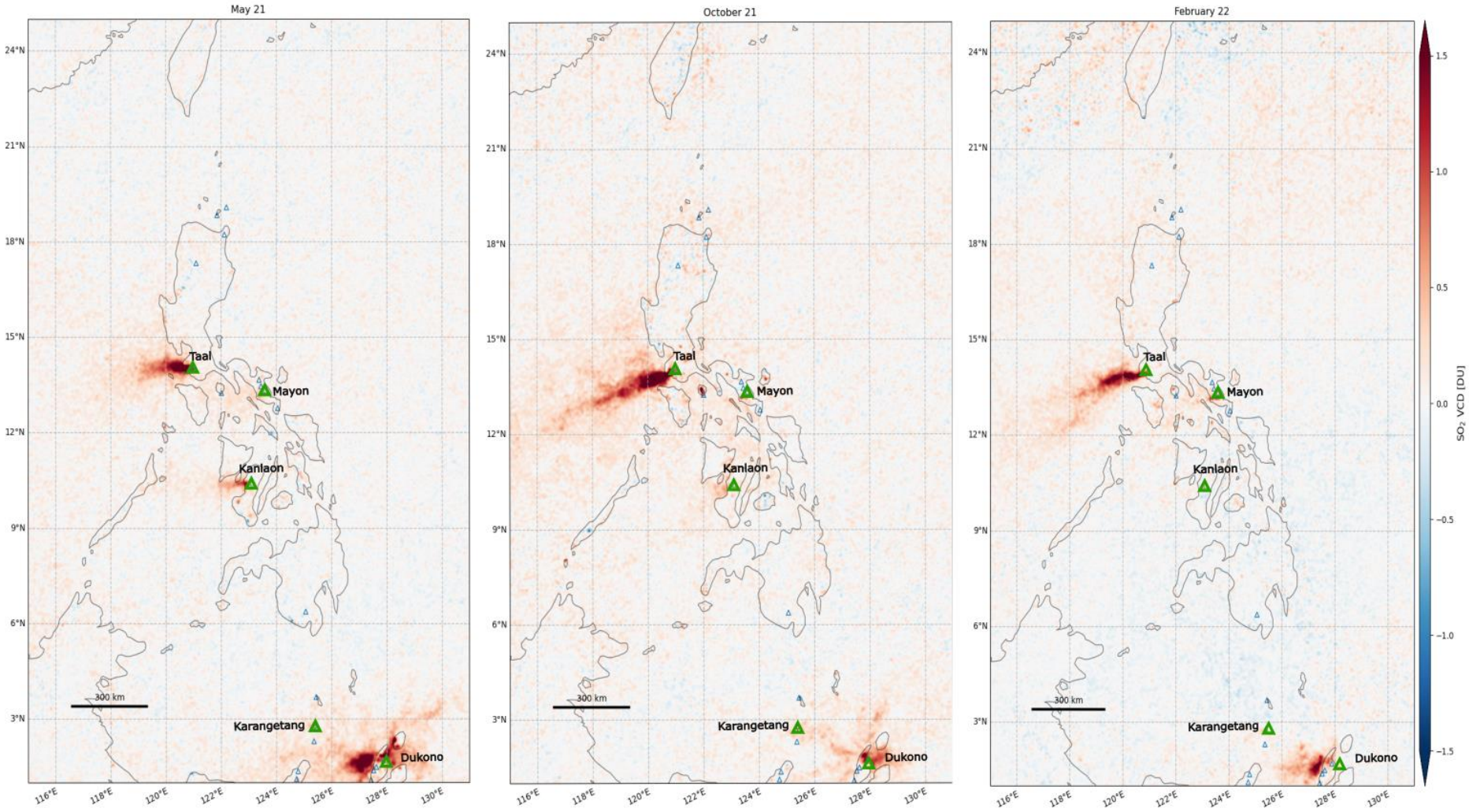

Figure 4.1. Regional maps of study area including distribution of volcanoes of interest and the monthly averaged SO_2 vertical column density (DU) for May 2021, October 2021, and February 2022.

4.3. Mass Eruption Rate and Sulphur Content ($S_{content}$)

The use of PlumeTraj provides not only the SO_2 emission rate but also the plume injection altitude, therefore is it possible to calculate both mass eruption rate (MER) and, subsequently, the magmatic S concentration, $S_{content}$. MER and injection altitude are empirically related according to equation (a) from Mastin et al. (2009):

$$MER = (\frac{H}{0.3035})^{4.15}$$

where *MER* is the mass eruption rate (kg s^{-1}), and *H* is the plume injection altitude above the vent (km). 0.3034 and 4.15 originates from the Mastin fit (Figure 4.2), where (1/0.241) = 4.15. The original $S_{content}$ in uncrystallised melt can then be calculated as a ratio of the emitted sulphur and the total tephra MER as equation (b):

$$S_{content} = \frac{\Phi(SO_2) \cdot r}{MER} \times 10^6$$

where $S_{content}$ is the sulphur content of the magma (ppm), $\Phi(SO_2)$ is the SO_2 emission rate (kg s^{-1}), *r* is the mass ratio of S to SO_2 (0.5005), and *MER* is the mass eruption rate (kg s^{-1}). It is important to note that the equation assumes an uncrystallised melt, which may not relate crystal content of Taal's magma. Analysed deposits from Taal 2020 eruption indicate a strong likelihood that the magma during that eruption was more andesitic (Balangue-Tarriela et al., 2022). Andesitic material has a porphyritic texture, which is obtained through the combining and cooling of magmatic material and volatiles (including sulphur) producing a series of minerals such as plagioclase feldspar and amphibole seen within the igneous rock (Moune et al., 2009).

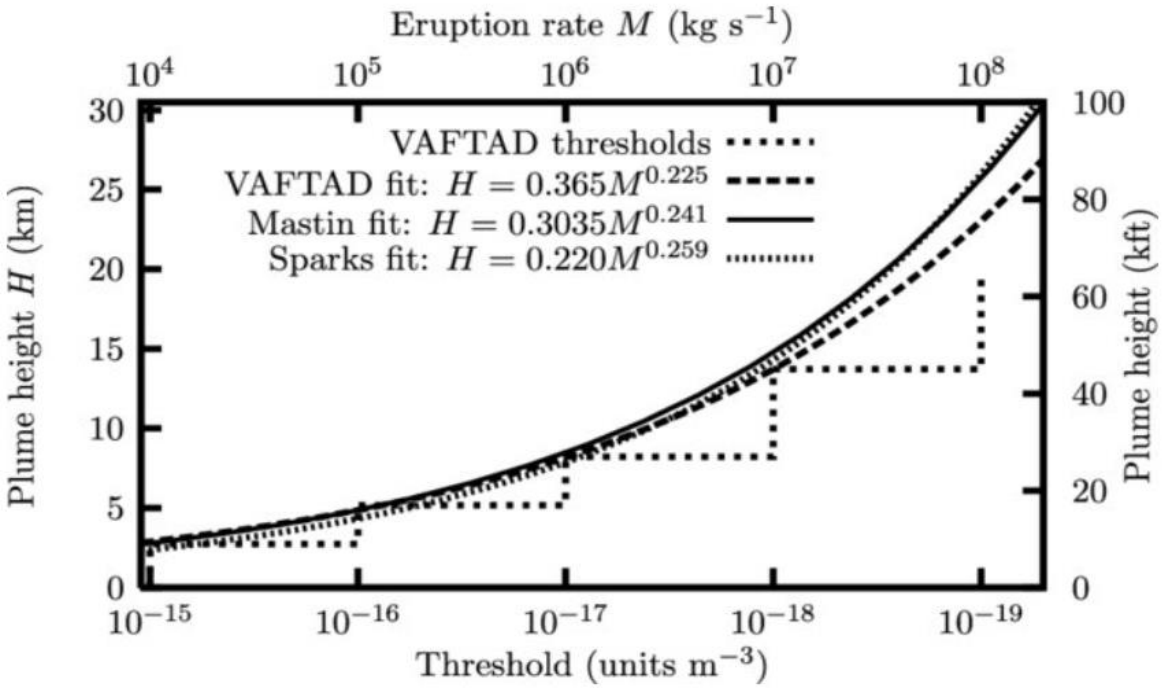

Figure 4.2. A comparison of estimates of eruption rate (M) as a function of the plume rise height H above the vent. This model includes estimates made by Sparks et al. (1997) and by Mastin et al. (2009) (From Webster et al., 2012).

Chapter 5. Results

5.1. Taal 2020 Eruption

These results will provide insights into eruption of the January 2020 Taal eruption by using the measured SO_2 from two orbits passing from 06:00 11/01/20 to 06:00 14/01/20 (all times given in UTC, PHT - 8 hours). PlumeTraj was used in conjunction with TROPOMI covering two days (12/01/20 and 13/01/20). Figure 5.1 shows SO_2 VCD, plume age and plume altitude for both days. From these images, a reconstruction of emission history has been made up to the time of overpass, before and during the eruptive phase (Figure 5.2). From the emission history, the measured SO_2 gas can be used in conjunction with plume height to work out the mass eruption rate, SO_2 emission rate, and $S_{content}$. VCDs are reported in Dobson units (DUs; 1 DU = 2.69 x 10^{16} molecules cm^{-2}) (NASA, 2023). Plume heights are derived from the SO_2 flux series (Figure 5.2) throughout various stages of the eruption.

The results show three separate injection altitudes of 2.5 km, 12.8 km, and 18.5 km on the 12/01/20 (Figure 5.2). These plume heights can be categorised into three separate phases of the eruption. The overpass on 12/01/20 was received ~04:50 13/01/20, approximately 24 hours after the eruption began and showed injection time from 06:00 11/01/20-06:00 13/01/20. The overpass on 13/01/20 captured the initial explosion as it drifted north-eastward (Figure 5.1).

Discontinuous degassing can be seen as early as 06:00 11/01/20 throughout the duration of the pre-eruptive phase at an altitude of 2.5-3 km (Figure 5.2). The eruption begins at approximately 05:00 (13:00 PHT) 12/01/22 as a steam-laden tephra column erupts from the main vent hitting an altitude of 18 (± 0.2) km. A second injection of SO_2-rich material is seen at 09:00 (17:00 PHT) reaching an altitude of ~12.5 (± 3) km increasing the SO_2 emission rate to a peak of 6102.98 (± 1557.15) kg s^{-1}. The south-westerly winds elongate the plume, diverting the column >1800 km NE overshadowing the small Japanese islands of Okinawa. The age of the main plume varies anywhere between <10 hours close to the volcano and ~12 hours further (Figure 5.1C). The third, lower injection altitude can be seen around 2.5 (± 0.3) km, with a direction of travel SW of Taal completely covering Occidental Mindoro, an island toward the south of Manila, Luzon. The 2.5 km injection appears to have the youngest gas emitted from the volcano (0-5 km) but toward the south increases to 20-30 hours, indicating that pre-eruptive gas may be incorporated within this plume. A period of lessened activity

begins between 18:00 and 22:00 (12/01/22), with SO_2 emission rate falling to 900 kg/s. A fourth injection of SO_2 gas seen between 23:00 (15:00 PHT) (12/01.20) to 01:00 (13/01/22) with a recorded SO_2 emission rate at 3600 (± 400) kg s^{-1} at an altitude 9-11 km. The total SO_2 mass for 12/01/20 was 1.76 (± 0.6) x 10^8 kg with a peak emission rate of 6102.98 (±1557.15) kg s^{-1} at 15:00 (23:00 PHT). Cloud fraction averaged 55% for the day.

The overpass on 13/01/20 was received ~04:35 14/01/20, approximately 48 hours after the eruption began. The overpass captured the ongoing explosive degassing and showed the original plume to the northeast (Figure 5.1). Due to the proximity of the swath edge, no SO_2 was detected from 06:00 to 15:00 12/01/20 (Appendix C). Into the early hours of 13/01/20, activity appears to decrease significantly from the previous unrest with the degassing SO_2 rates fluctuating from 100 - 500 kg s^{-1} (Figure 5.2). A fifth and final injection of SO_2 is seen at 10:00 (02:00 PHT) 13/01/20 with plume height increasing from 10 km to 13.5 km. The total SO_2 mass on 13/01/20 was 2.95 (±0.96) x 10^7 kg with a peak emission rate at 1474.25 (±303.72) kg s^{-1} at 13:00 (05:00 PHT) 13/01/20. The eruption ended on 22/01/20. Cloud fraction averaged 46% for the day.

Table 5.1. Average and peak SO_2 emission rates with pre-eruptive magma $S_{content}$ for the explosive activity at Taal volcano

Date	Injection Altitude (km)	MER (x 10^6 kg s^{-1})	Average SO_2 Emission Rate ($kg \cdot s^{-1}$)	Average $S_{content}$ (ppm)	Peak SO_2 Emission Rate ($kg \cdot s^{-1}$)	Peak $S_{content}$ (ppm)
12/01/20	12.8 (± 1.4)	5.55 (± 3.1)	2833 (± 1711)	257 (± 134)	6102 (± 1793)	550.37 (± 134)
13/01/20	12.06 (± 1.6)	4.33 (± 2.4)	571 (± 430)	69.15 (± 196)	1474 (± 411)	91.77 (± 34)

5.1.1.; Mass Eruption Rate (MER) and Sulphur Content ($S_{content}$) Calculations

The MER and $S_{content}$ was calculated using equation (a) and (b) for the average SO_2 emission rate and average plume height (km) and the peak SO_2 and corresponding plume height during the peak emission rate across both days.

Calculated average MER:

12/01/20 $\frac{12.8}{0.3035}^{4.15} = 5.55 \times 10^6$ kg s^{-1}

13/01/20 $\frac{12.06}{0.3035}^{4.15} = 4.33 \times 10^6$ kg s^{-1}

Where 0.3015 and 4.15 relates to the Mastin fit (Figure 4.2) and 12.8 km and 12.06 km are the average plume heights for both days.

Calculated average $S_{content}$:

12/01/20 $\frac{2833 \cdot 0.5005}{5.55 \times 10^6} \times 10^6 = 255.48\, ppm$

13/01/20 $\frac{571 \cdot 0.5005}{4.33 \times 10^6} \times 10^6 = 66\, ppm$

Where 2833 kg s^{-1} and 571 kg/s are the average SO_2 emission rates, 0.5005 is the mass ratio of S to SO_2, 5.55 x 10^6 kg s^{-1} and 4.33 x 10^6 kg/s are the average MER, and x 10^6 is the unit conversion to parts per million (ppm).

Calculated peak MER:

12/01/20 $\frac{12.8}{0.3035}^{4.15} = 5.55 \times 10^6$ kg s^{-1}

13/01/20 $\frac{14}{0.3035}^{4.15} = 8.04 \times 10^6$ kg s^{-1}

Where 0.3035 and 4.15 relates to the Mastin fit (Figure 4.2) and 12.8 km and 14 km are the peak plume heights for both days.

Calculated peak $S_{content}$:

12/01/20 $\frac{6102.98 \cdot 0.5005}{5.55 \times 10^6} \times 10^6 = 550.37\, ppm$

13/01/20 $\frac{1474.25 \cdot 0.5005}{8.04 \times 10^6} \times 10^6 = 91.77\, ppm$

Where 6000 kg s^{-1} and 1500 kg s^{-1} are the peak SO_2 emission rates, 0.5005 is the mass ratio of S to SO_2, 5.55 x 10^6 kg s^{-1} and 8.04 x 10^6 kg s^{-1} are the peak MER, and x 10^6 is the unit conversion to parts per million (ppm)

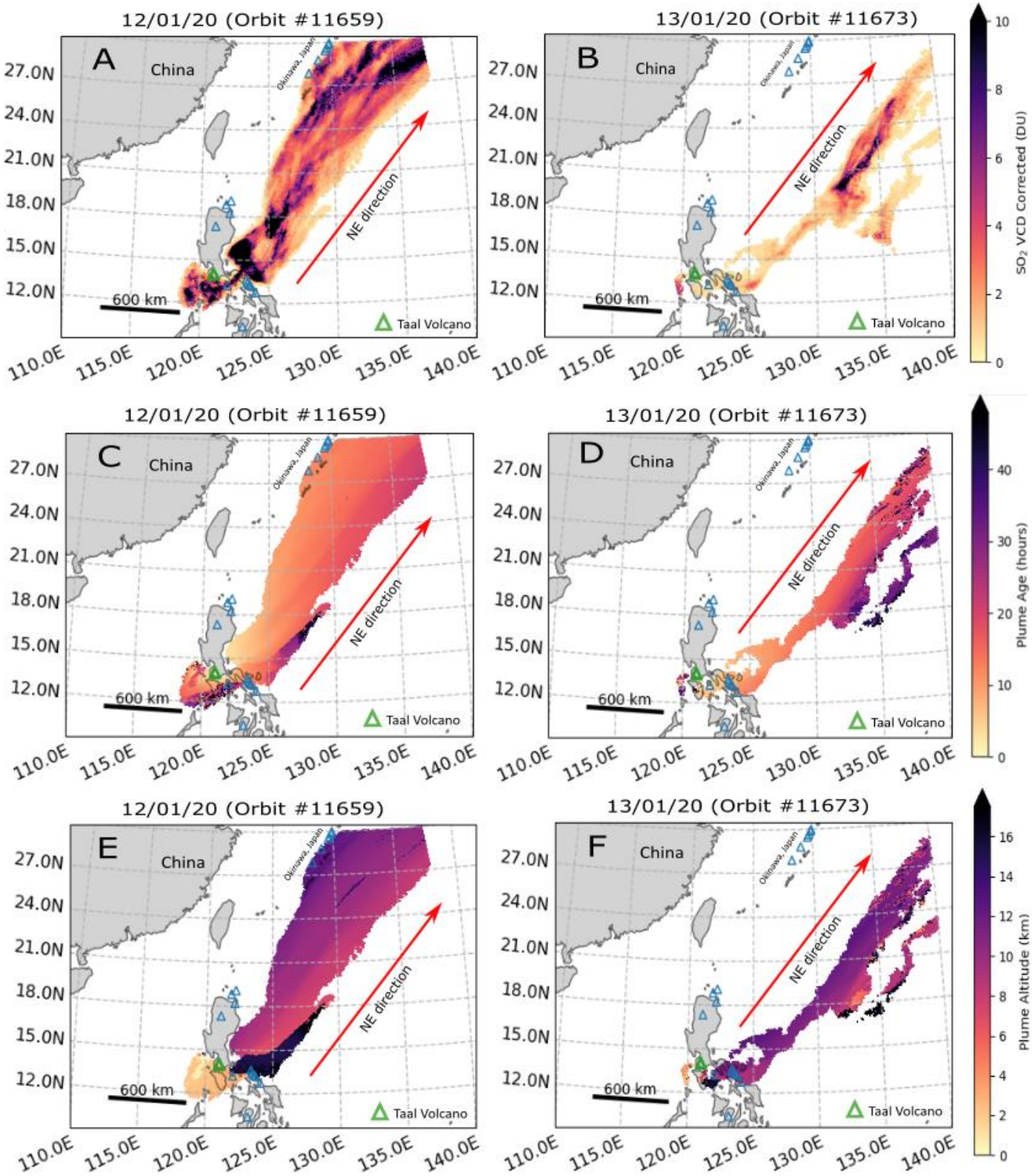

Figure 5.1. PlumeTraj received images using TROPOMI for January 2020 Taal eruption for 12/01/20 (left side) and 13/01/20 (right side). The figure displays corrected vertical column densities (VCD) of SO_2 (DU) (A and B). plume altitude in km (C and D), and plume age in hours (E and F).

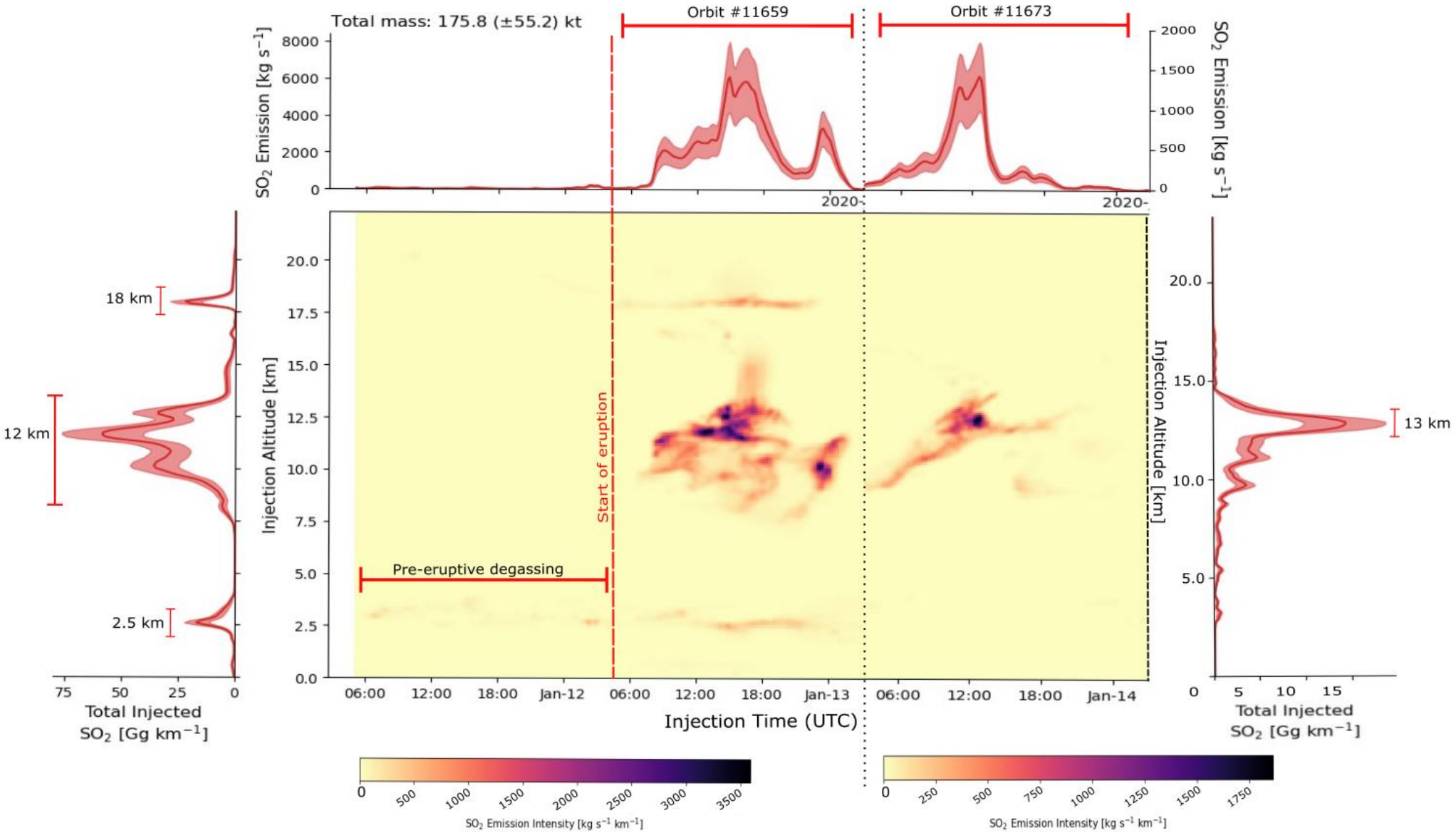

Figure 5.2. PlumeTraj received images using TROPOMI for January 2020 Taal eruption from 06:00 11/01.20 – 00:00 14/01/20. The figure shows SO_2 emission intensity of each overpass (injection time) whilst displaying corresponding injection altitude, total injected SO_2 and SO_2 emission. Dotted line is the boundary between both orbits used for the overall flux series (#11659 and #11673). Flux between 06:00 11/01/20 to 00:00 13/01/20 are shown on the left of orbit boundary with corresponding injection altitude, total injected SO_2 and SO_2 emission whilst data between 00:00 13/01/12 to 00:00 14/01/20 are shown on the right. Note that for both orbits, the SO_2 emission intensity and SO_2 emission are different scales.

5.2. Long Term Average SO_2 of Philippine and Indonesian Volcanoes

The results presented within this chapter help aid our understanding into the applications of TROPOMI and how the data can be used to investigate long term degassing patterns. All available data from the S5P was used until February 2022. By having access to this global archive of volcanic regions, it will enable the advancement of volcanic monitoring globally as well as providing access to remote volcanoes such as Kanlaon, Dukono and Karangetang. It also provides consolidation to pre-existing literature discussing the volcanic system as a whole through geological and geochemical studies for well-studied volcanoes such as Taal and Mayon. Figure 5.3 shows the daily SO_2 emissions per month (t day^{-1})

Taal's long-term degassing behaviour indicates a period of steady state from June 2018-April 2021, excluding the 2020 eruption, before entering a period of pulsating elevated degassing from May 2021-February 2022 (Figure 5.3). From June 2018-April 2021, daily SO_2 emissions averaged 256.16 ± 67.49 t day^{-1}, with a high of 370.15 t day^{-1} in April 2019 and a low of 144.48 t day^{-1} in September 2018. From May 2021-February 2022, daily SO_2 emissions increased to an average of 1139.3 ± 340.49 t day^{-1}, with a high of 1694.8 t day^{-1} in September 2021 and a low of 761.91 t day^{-1} in February 2022. The standard deviation highlights the high variability in emission rate due to the pulsating injection behaviour of Taal's degassing. The SO_2 emission rate for January 2020 was measured at 12.5 kt day^{-1} using this long-term averaging approach. No gas was detected for the months of July and August 2018; July, August, and September 2019; and August 2020, possibly a result of a back-trajectory analysis failure, high cloud coverage obscuring any SO_2 released and//or the SO_2 was too weak to be detected.

Mayon's and Kanlaon's long-term degassing profile indicates that both volcanoes were in a constant steady state period from June 2018-February 2022 (Figure 5.3). For Mayon, daily SO_2 emission averaged 247.86 ± 120.62 t day^{-1} from June 2018-February 2022, with a high of 596.28 t day^{-1} in January 2022 and a low of 3616 t day^{-1} in August 2020. For Kanlaon, daily SO_2 emission averaged 166.41 ± 95.5 t day^{-1} from June 2018-February 2022, with a high of 395.65 t day^{-1} in December 2020 and a low of 25.021 t day^{-1} in July 2019. Kanlaon has emitted the least amount of SO_2 from June 2018-February 2022 out of the five measured volcanoes.

Dukono's and Karangetang's long-term degassing profile indicates inconsistency and high fluctuating mass measurements from June 2018-February 2022 representing the volcanoes'

constant state of eruptive activity (Figure 5.3). For Dukono, daily SO_2 emission averaged 862.54 ± 302.41 t day^{-1} from June 2018-February 2022, with a high of 1610.3 t day^{-1} in August 2019 and a low of 241.02 t day^{-1} in February 2020. For Karangetang, daily SO_2 emission averaged 442.86 ± 284.25 t day^{-1} from June 2018-February 2022, with a high of 1000.4 t day^{-1} in July 2021 and a low of 29.59 t day^{-1} in February 2020. Both profiles of the volcanoes show similarity with regards to daily SO_2 emissions per month with consistency in similar periods of increased and decreased activity.

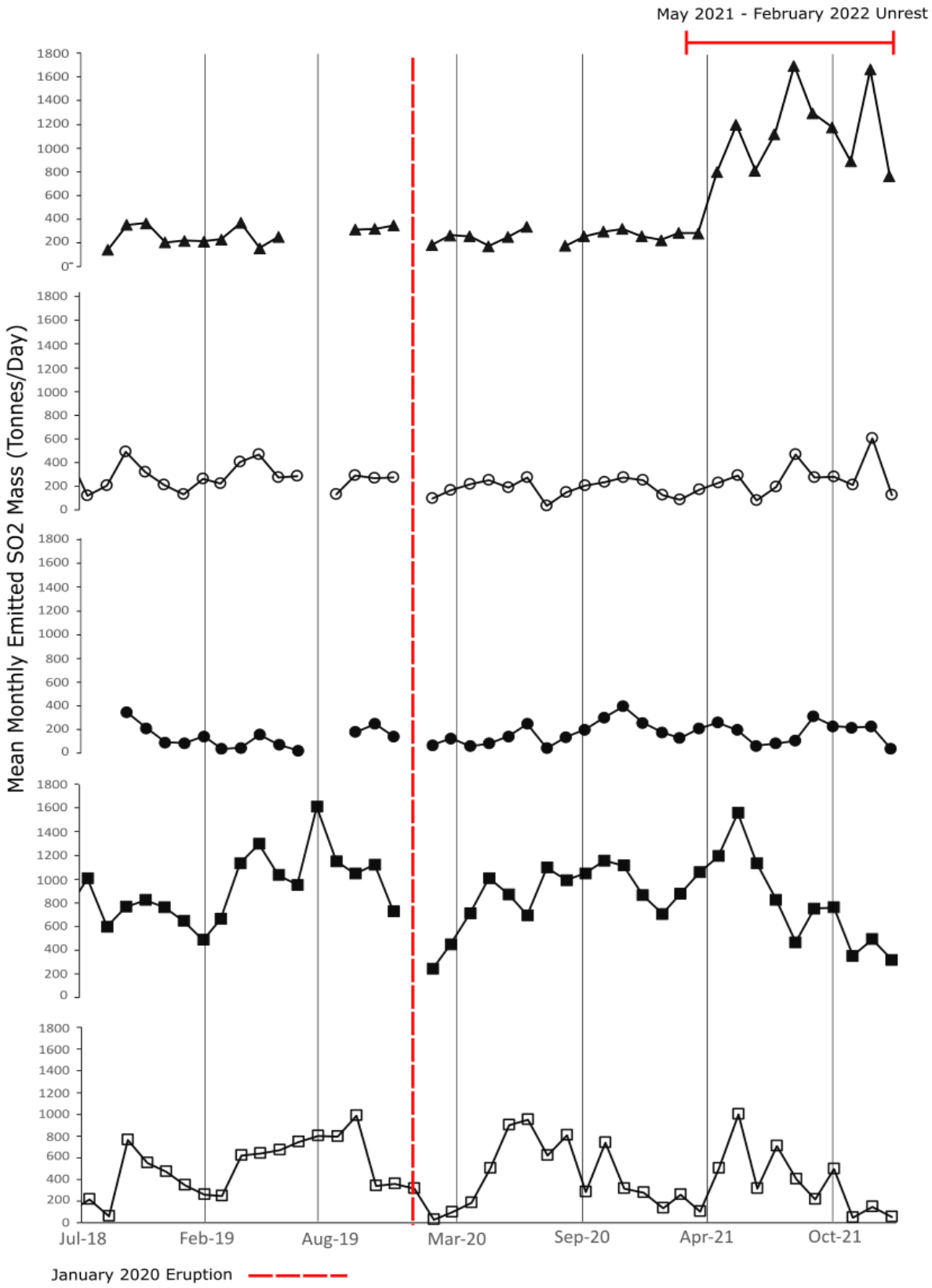

Figure 5.3. Mean monthly emitted SO_2 mass (t day^{-1}) series from June 2018 to February 2022 for (a) Taal (▲), (b) Mayon, (○), Kanlaon (●), and (c) Dukono (■), and Karangetang (□). SO_2 data retrieved from TROPOMI using PlumeTraj where 1 km vertical column densities were converted into SO_2 mass using formula A. SO_2 mass values are a representation of the average monthly SO_2 mass in each designated volcanoes vicinity (Appendix A).

Chapter 6. Discussion

6.1. Flux through time

During the progress of the eruption, the total SO_2 peaked twice, once on both days of the overpass (12/01/12-13/01/12). The first peak was seen when the confirmed eruption took place at approximately 13:00 PHT with a peak emission rate of 6102 (±1793) kg s^{-1} at 15:00 PHT 12/01/20. The total SO_2 mass for the day of 12/01/20 was 1.76 (± 0.6) x 10^8 kg and the peak mass eruption rate was 5.55 (± 3.1) x 10^6 kg s^{-1}. The second peak occurred on the following day (13/01/20) with a peak emission rate of 1474 (± 411) kg s^{-1}, approximately a quarter of what the initial eruption emission rate the previous day was. The peak mass eruption rate for 13/01/20 was 4.33 x 10^6 kg s^{-1}. The decrease in activity throughout the two days, shows that the eruption is fuelled by a depleting magmatic injection and the bulk of the degassing period has spanned across both days. Without the introduction of magmatic recharge, the eruption will be short-lived, relying only on the material supplied from the initial magmatic injection on 12/01/20.

Using Table 2.1, a total SO_2 mass of >10^8 would be fitting for a VEI equal 3. However, the size of both the vertical eruptive column and umbrella cloud for the 2020 eruption agrees with a VEI equal to 4. Our earlier inference that the VEI of the eruption was equal to 4 was based on the umbrella cloud and vertical eruptive column alone. There is a degree of bias when allocating the VEI to an eruption when the values do not all correlate to a single category. An explanation for a MER smaller than what you would expect to see from a VEI equal to 4 may be a consequent of limitations of the application used to measure, in this case TROPOMI. Cloud coverage is high within SE Asia due to the high moisture content (Taisne et al., 2019), a factor which affects the SO_2 signal retrieved by the satellite. Average cloud cover across northern Philippines can be anywhere between 35 – 50 % for January (WeatherSpark, 2020). The cloud fraction across the duration of the eruption saw large areas of pixels that were completely covered in cloud leading to an overall average cloud cover of 55%.

6.2. Injection altitude

The altitude to which the gas was injected varied between three different heights: 2.5 km, 12 km, and 18 km. The bulk of SO_2 ranged between 10 km to 13 km and dispersed towards the NE at the same altitude it was erupted at. The small plume lower in altitude towards the

WSW of Taal is a product of the material injected at 2.5 km. Some of this material can be attributed to the pre-eruption degassing, which is SO_2 poor indicating that this layer is predominately steam generated from the hydrothermal reservoir and main crater lake due to the interaction of magma and water (Yamaya et al., 2013). However, the vent altitude was significantly lower than the injection altitude of this material, which was released before the eruption began. An explanation for this discrepancy is due to the plume buoyancy increasing as a result of the thermal emission from the magmatic intrusion rapidly accelerating the movement of material into the atmosphere (Carey and Burski, 2015). To prove this theory, a secondary research project must investigate the pre-eruptive thermal flux from Taal using either MODIS or MODVOLC.

From 13:00 PHT another injection of material is seen, confirmed by PHIVOLCS (2020) to be predominately steam-driven through use of Synthetic Aperture Radar (SAR) analysis. It is probable that this plume had generated from the groundwater and lake, hence why at 18 km there is a poor SO_2 flux at that altitude. Although PHIVOLCs report that the first plume of activity seen reaches ~10 km, our results show that SO_2 was detected up to 18 km, indicating either the force of the first eruption was enough to send material higher than previously thought or the heat from the magmatic intrusion increased the plume buoyancy through interaction with the hydrothermal system. The first signs of phreatomagmatic activity were not seen until 13:00 PHT, in which the second injection of SO_2 rich material was introduced into the atmosphere. The bulk of the SO_2 detected was during this second injection, indicating that the deflation of the magma fuelling the eruption had begun. Comparing with the infrasound (17 km) and other TROPOMI SO_2 retrievals (20 km), the maximum plume height was detected at ~18 km (Perttu et al., 2020; Bachmeier et al., 2020). Some SO_2 feedback can be noticed at altitudes of up to 20 km but the SO_2 mass is small in comparison to the bulk of the SO_2 received between 12-15 km. It is likely that the SO_2 signal at >18 km is a product of heat discharge from the eruption increasing volatile buoyancy into the atmosphere. The calculated average plume height for 12/01/20 was 12.8 ± 1.4 km.

6.3. Magmatic Sulphur Content ($S_{content}$)

Our results show that the magmatic $S_{content}$ was higher during the pre-eruptive phase (550.37 ppm) than the post-eruptive phase (91.77 ppm), indicating that the bulk of the gaseous sulphur derived through gas-melt segregation during its ascent had already been degassed throughout the first day of the eruption (Edmonds, 2008). Basaltic-andesitic magmas, like

Taal, are known to exsolve gases more readily than highly silicic magmas, a result of the low viscosity allowing gaseous movement and easier gas-melt segregation (Sparks, 2003; Edmonds, 2008). Both gas exsolution and segregation are fundamental variables on eruption dynamics and magma genesis (Sparks, 2003). The stark contrast of $S_{content}$ between 12/01/20 and 13/01/20 provides an insight into the eruption dynamics, implying only one magmatic injection providing fresh dissolved gas within the melt was seen throughout the eruption. If another injection of magma were seen, there would have been increased activity, creating a change in PHIVOLCS alert level from 4 to 5, and a higher calculated $S_{content}$ from 13/01/20. Fortunately, no magmatic recharge was seen throughout the duration of the eruption, which is possibly the likelihood of PHIVOLCS only raising the alert level to 4. The concluding remarks were that the eruption was indeed a phreatic eruption between heat from the magma and steam from the hydrothermal reservoir and main crater lake (PHIVOLCS, 2020).

Our results can also provide an understanding of Taal's profile through a comparative analysis of other volcanoes of similar tectonic setting and magma composition. Shinohara's (2008) comprehensive study on the excess degassing of volcanoes examined multiple papers and created a complex table investigating the relationships of $S_{content}$ in melt inclusions, glass matrix, and total concentration using petrological samples. Table 7.1 shows average $S_{content}$ values for both subduction and non-subduction volcanoes and volcanoes that are dacite- and andesite-only in composition. These values make it possible to put the eruption into the wider context of other similar explosive events, showing that the $S_{content}$ calculated on 12/01/20 was slightly above the calculated average of other subduction volcanoes, possibly a factor of the incorporation of highly silicic subducted terrigenous material from the South China Sea (Mukasa et al., 1994; Castillo and Newhall, 2004). The introduction of the terrigenous material plays a significant role in the geochemical signature of arc lavas, contributing to the isotopic variability and silica content in the melt (Mukasa et al., 1994; Castillo and Newhall, 2004; DuFrane et al., 2006). However, the standard deviations imply that there is a striking variability in the $S_{content}$ seen throughout both volcano types.

Table 6.1. Average $S_{content}$ (ppm) from petrological samples from 24 explosive eruption events at both non-subduction and subduction zones and volcanoes whose magma are dacite- and andesite-only (Adapted from Shinahawa, 2008). Right side shows Taal 2020 eruption calculated $S_{content}$ (ppm) for 12/01/20.

	Non-subduction	Subduction	Dacite-only	Andesite-only
S in melt inclusion	1186.57 ± 678.7	463.88 ± 685.17	136.2 ± 89.74	582.8 ± 294.07
S in matrix glass	230.71 ± 161.72	99.53 ±89.85	62.2 ± 33.12	69.4 ±21.95
ΔS	955.86 ±655.36	363.35 ± 620.9	74 ± 66.92	513.4 ± 305.77

Taal 2020 Eruption

Date	Average $S_{content}$ (ppm)	Peak $S_{content}$ (ppm)
12/01/20	257 (± 134)	550.37 (± 134)
13/01/20	69.15 (± 196)	91.77 (± 34)

6.4. Pre-Eruptive Phase Taal

Prior to the 2020 eruption, Taal's behaviour was stable, but the volcano has been known in the past to be unpredictable regarding a sudden change in unrest normally associated with a series of seismic crisis or ground inflation (Arpa et al., 2013; Hernandez et al., 2017; Zlotnicky et al., 2018). Evaluating the activity seen from Taal, Mayon, and Kanlaon (Figure 6.1), there is a noticeably similar pattern in regard to the daily SO_2 emission per month (t day^{-1}) especially across Taal and Mayon. PHIVOLCs released a press statement addressing public concerns that the three volcanoes were synchronised regarding their activity, to which they announced that the activity is just a "coincidence" as they were "all active volcanoes" that were "very far from each other" (ABS-CBN News, 2021).

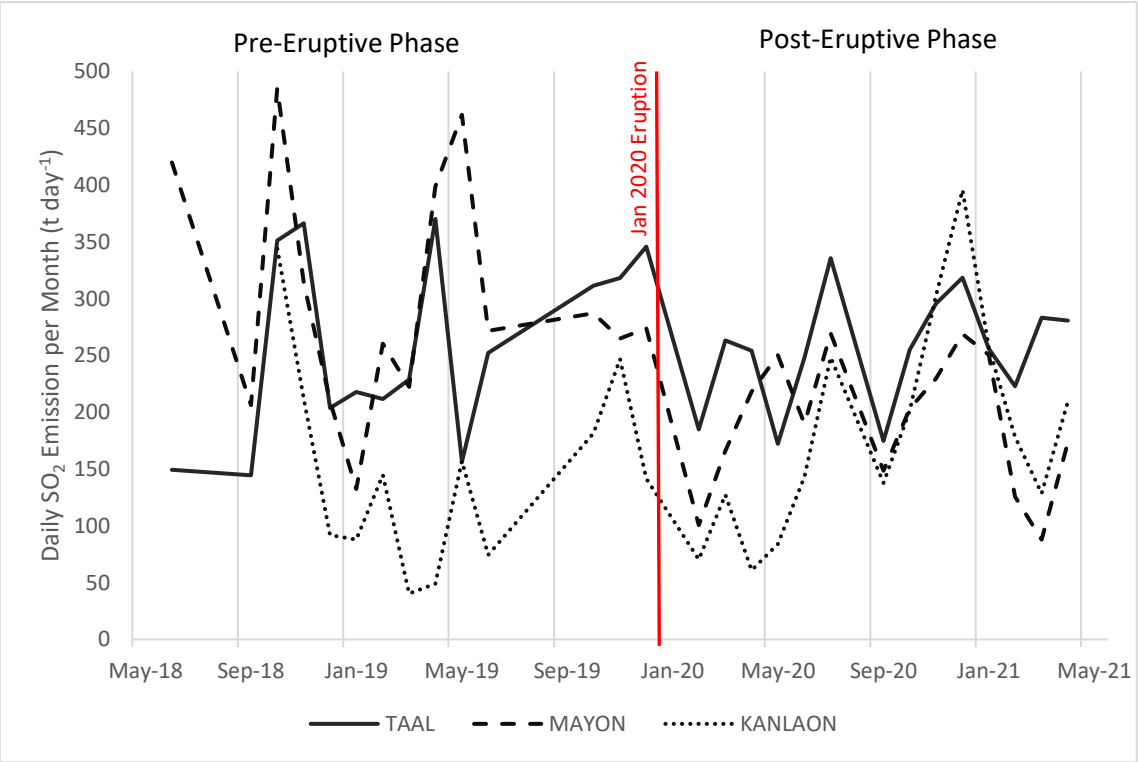

Figure 6.1. Daily SO_2 emission per month (t day^{-1}) from June 2018-April 2021 for Taal, Mayon and Kanlaon. January 2020 serves as boundary between Taal's pre- and post-eruptive phase. Values for January 2020 were not included.

During the lead up to the eruption, Taal's daily SO_2 emission peaks in October 2018 (351 t day^{-1}), November (366 t day^{-1}), and April 2019 (370 t day^{-1}). Following the release of SO_2 in April 2019, the gas released halves in May 2019 (156 t day^{-1}) before steadily building up throughout the remaining months to the 2020 eruption, reaching a maximum 345 t day^{-1} in December 2019. The building phase may provide some insight into the magmatic behaviour identifying the strain that was taking place due to the fresh magma injection into Taal's hydrovolcanic system. The time of the build-up may also be crucial; 6 months of no sudden release of material was observed by PHIVOLCS towards the end of 2019. Figure 6.2 visualises the peaks in which SO_2 was suddenly released highlighting that daily SO_2 emission almost doubles in a short period of time (1-2 months) before halving within a similar time frame. The slow increase in emission rate prior to the eruption may be an additional precursor to the 2020 eruption that was seen the following year. Other precursory events occurring within the Taal Caldera have been noted for years prior to the eruption. PHIVOLCS found that using continuous global positioning surveys (GPS) across the Taal region, there had been a slight inflation beginning January 2019 relative to November 2018 (PHIVOLCS, 2019). By combining GPS with precise levelling measurements across the volcano, they found that the

inflation continued up until the eruption, with indications of slight inflation found in March 2019, June 2019, and September 2019 (PHIVOLCS, 2019). A study investigating CO_2 degassing as a precursor to the eruption found that there had been significant temporal variations spanning across ~12 years reaching high degassing rates in 2011 and 2017 (Pérez et al., 2022). Their work found that the CO_2 signals represent a magma recharge within this time period, a possible early precursor to the January 2020 eruption.

6.5. Post-Eruptive Phase Taal

After the January 2020 eruption, Taal's activity returned to normality similar to before the eruption. The immediate months after the eruption saw Taal's daily SO_2 emission drop from 1052 t day^{-1} to 185 t day^{-1}. From February 2020 to April 2021, Taal's total SO_2 mass averaged 253 ± 50 t day^{-1}. However, from May 2021, Taal's activity began stirring again to what was seen as an episode of unrest with occasionally eruptive activity. Figure 6.2 shows Taal's pre- and post- unrest phases from February 2020 to February 2022 with comparison to the activity seen in Mayon and Kanlaon. PHIVOLCS (2021) reported signs of activity from Taal from as early as March 2020, as GPS showed increased ground deformation towards the NW sector of the caldera. Increased daily SO_2 emissions were first seen in May 2021, though signs of activity through changes in the lake's geochemistry were seen prior in February 2021, as pH changed from 2.79 to 1.59 (January 2020 measurement) (PHIVOLCS, 2021). During the post-unrest phase, three distinct peaks of heightened activity were seen in June 2021 (1194 t day^{-1}), September 2021 (1694 t day^{-1}), and January 2022 (1663 t day^{-1}). The TROPOMI observations show a parallel between peaks in SO_2 and peaks in eruptive behaviour that were observed. The peaks correspond to several phreatomagmatic bursts that were seen throughout July 2021, November 2021, and January 2022. However, to put into context, using Figure 5.3 daily SO_2 emission per month (t day^{-1}) for the January 2020 eruption was 2.44 x 10^5 t day^{-1} (2833 kg s^{-1}), more than an order of magnitude larger than the peak emission of 2021 unrest. Though the unrest period may be an act of magmatic recharge, it does not equate to the intensity of the magmatic injection seen prior to the January 2020 eruption thereby suggesting a minor recharge of Taal's magma source.

Table 6.2. SO_2 emission rate (t day^{-1}) for Taal, Mayon, Kanlaon, Dukono, and Karangetang for 2018-2021 with total mean. Values were calculated using averaged daily SO_2 emission rate for each month (Figure 5.3). For comparison, Carn et al.'s (2017) results using OMI were added.

	Daily SO_2 Emission (t day^{-1})					
	2018	2019	2020	2021	Mean	Carn et al., (2017)
Taal	243 ± 108	286 ± 71	250 ± 58	834 ± 486	399 ± 393	-
Mayon	317 ± 143	272 ± 97	189 ± 73	221 ± 104	250 ± 109	453
Kanlaon	237 ± 107	115 ± 71	165 ± 111	187 ± 77	176 ± 95	70
Dukono	769 ± 126	988 ± 316	852 ± 297	877 ± 326	872 ± 291	1726
Karangetang	393 ±269	566 ± 247	493 ± 329	371 ± 273	456 ± 280	313

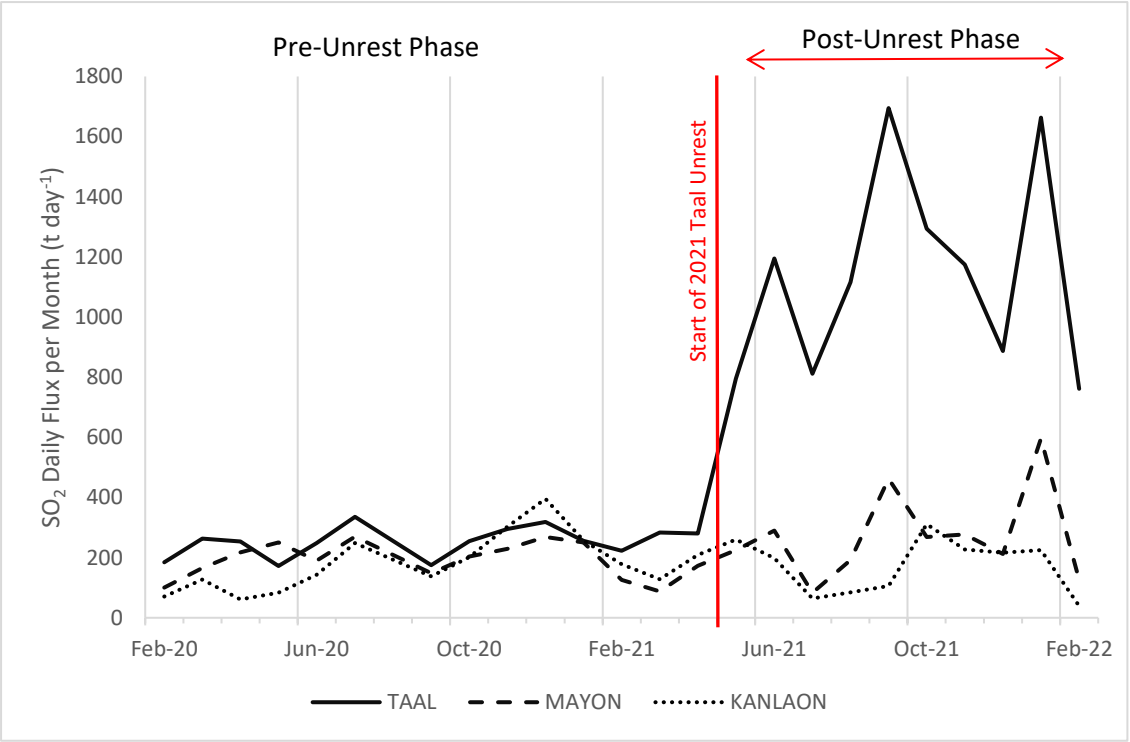

Figure 6.2. Daily SO_2 emission per month (t day^{-1}) from February 2020-February 2022 for Taal, Mayon and Kanlaon. April 2021 serves as boundary between Taal's pre- and post-unrest phase.

6.6. Mayon and Kanlaon Activity

Mayon and Kanlaon are the lowest emitters of SO_2 across the region. Within the study Mayon's SO_2 fluctuated between 30-600 t day^{-1} with a mean SO_2 emission rate of 250 ± 109 t day^{-1}. Carn et al. (2017) found Mayon's average SO_2 emission between 2005-2015 was 453 t day^{-1}. Kanlaon's SO_2 fluctuated between 25-400 t day^{-1} with a mean SO_2 emission rate of 176 ± 95 t day^{-1}. Carn et al. (2017) found Kanlaon's average SO_2 emission between 2005-2015 was 70 t day^{-1}. Between 2018-2022, Mayon appeared less active whilst Kanlaon appeared more active than what had been previously seen across Carn et al.'s study. An explanation could be the level of recharge of the mafic magma, which supplies volatiles through mixing and mingling of fresh injected magma (Wallace et al., 2015). However, the results indicate that the recharge of Kanlaon was not enough to cause any eruption, though PHIVOLCS reported steam plumes with SO_2 emissions varying 116-237 t day^{-1} between June-July 2020. SO_2 emissions for June-July 2020 from Figure 5.3 were 143 t day^{-1} and 248 t day^{-1}, respectively. Peaks in Mayon's activity (Figure 5.3) in July 2018, October 2018, May 2019, September 2021, and January 2022 coincide with observational reports by PHIVOLCS including plume generation varying between white-grey and some lava effusion. PHIVOLCS

additionally reported a distinctive drop in activity in comparison to the normal background activity typically seen in Mayon (~ 500 t day^{-1}). In July 2019, SO_2 emissions dropped to average 156 t day^{-1}. Figure 5.3 finds that daily SO_2 emission for 2019 were 272 ± 97 t day^{-1}, though higher in value it is still relatively low against Mayon's baseline (~ 500 t day^{-1}).

6.7. Dukono and Karangetang Activity

Dukono is the biggest emitter of SO_2 across the region, complimenting the literature that Dukono is a big contributor to volcanic SO_2 emissions across the world (Carn et al., 2017; Bani et al., 2018). Within this study, Dukono's SO_2 fluctuated between 240-1550 t day^{-1} with a mean SO_2 emission rate of 872 ± 291 t day^{-1}. Comparing with Bani et al.'s (2018) study using DOAS, Dukono's SO_2 emission fluctuated between 400-2000 t day^{-1} with a mean SO_2 emission rate of 819 ± 235 t day^{-1}. Carn et al. (2017) found Dukono's average SO_2 emission between 2005-2015 was 1726 t day^{-1}. Karangetang's SO_2 fluctuated between 30-990 t day^{-1} with a mean SO_2 emission rate of 456 ± 280 t day^{-1}. Carn et al. (2017) found Karangetang's average SO_2 emission between 2005-2015 was 313 t day^{-1}. The results show that both volcanoes have been releasing a significant amount of SO_2 for over 15 years. Karangetang and Dukono's activity is accredited to the arc-arc collision of the Molucca Sea Plate and the presence of the I-MORB mantle underneath (Morrice and Gill, 1986; Macpherson et al., 2003; Bani et al., 2018). Dukono's volcanism is sustained by a depleted I-MORB mantle source, which has been undergoing lateral pressure from its geological situation, leading to high fluid fluxes toward the surface (Bani et al., 2018). Although the Sangihe arc (Karangetang) is influenced by the I-MORB, the lava seen across the arc are consistent with the sediment signature from the upper North Sulawesi plate. The findings from this study implies that the Molucca Sea Plate remains an active plate margin that influences the activity at both Karangetang and Dukono. Degassing of the I-MORB through diffusion and decompression and the collided accretionary wedges under the Sangihe arc is the likely factor of the SO_2 fluxes seen at both volcanoes (Bottinga and Javoy, 1990; Macpherson et al., 2003; Aubry et al., 2013; Bani et al., 2018).

Both Dukono and Karangetang have been categorised by MAGMA as level II volcanoes, where the results show both visual activity and instrumental observations signalling an imminent eruption. Dukono and Karangetang showed visual activity in the form of white-ash plumes extending anywhere between 100 m to 3 km during periods of heightened activity. In 2018, Dukono's activity averaged at least 5 reports of ash plumes per month with altitudes

ranging between 1.4-2.1 km (Global Volcanism Program, 2023). PVMBG reported an increase in both plume generation and plume height from April-September 2019. Figure 5.3 shows a peak in SO_2 emission during the same period, with the highest daily SO_2 emission (t day^{-1}) in August (1610 t day^{-1}). From September 2019-February 2020, the volcano overall more visible with some days of fog surrounding the vent until plume generation increased from March 2020 to October 2020 varying around 0.1-0.9 km. The peak plume during this period (Mar-Oct 2020) was during October which coincides with the peak SO_2 emission recorded (Figure 5.3) at 1097 t day^{-1}. Volcanism generally increases with plume generations between 0.1-0.7 km during June 2021, where we see an increase output of SO_2 emission at 1556 t day^{-1}. From July 2021-February 2022, Dukono's activity lessens, and plume height varies around 0.025-0.3km above vent altitude with frequent days being plume-free (MAGMA). This decrease in visual activity seen around Dukono coincides with the decrease seen in SO_2 emission dropping from 1132 t day^{-1} (July 2021) to 317 t day^{-1} (February 2022).

Observational reports for Karangetang (PVMGB and Darwin VAAC) found that there has been a build of seismicity and thermal anomalies since November 2018. From Nov 2018, activity began increasing from February 2019 with continuous lava flow effusing from the crater edifice from February 2019-April 2020. During this period, SO_2 emissions fluctuated between 30-985 t day^{-1}. February 2019 daily SO_2 emissions per month was 29.6 t day^{-1}, contradicted the observational reports of continuous lava flows and ash plumes reaching 0.2 km. However, PVMBG reported that observational reports were prevented due to poor weather conditions including fog, which may be a limiting factor affecting the SO_2 retrieval by TROPOMI. From April-October 2019, PVMBG reported a continuous eruption consisting of avalanches of material travelling up to 1.8 km down adjacent drainages alongside steam-ash plumes varying anywhere between 0.3-7.6 km. The eruption continued until February 2021 where no further observational reports were taken between March-November 2021, though daily SO_2 emission varied between 100-1000 t day^{-1}, peaking in June 2021 (1000.4 t day^{-1}).

6.6. Limitations and Future Research

There are several key themes on the shortcomings of this study. The first being limited access to the PHIVOLCS volcano data repository for the region's volcanoes including Taal, Mayon and Kanlaon. Though connections were attempted, no response was received from PHIVOLCS and therefore only public datasets were used. A second limitation was the methodological approach. The averaging approach was quite simple and did not take account of wind direction. A better approach would be to develop a code which can outline returned pixels as close to the volcano as possible as there was no way to identify what SO_2 belonged to which volcano, especially if the plumes crossed path (e.g., Karangetang and Dukono). Hand-drawn boxes around each volcano to calculate the daily SO_2 emission per month (t day^{-1}) for each volcano allows error in regard to both underestimation and overestimation of SO_2 for each volcano. If the study were to be repeated, my suggestions would be having a daily measurement of SO_2 separately to the monthly average to improve the quality of the datasets and for better insights into the volcanic profiles.

Regarding the 12th January 2020 Taal eruption, the main limitation with the dataset is the time-scale. The duration of the eruption began on 12/01/20 and lasted till 22/01/20. If the study were repeated, my suggestions would be to create a time flux series from 09/01/20 to 25/01/20 to incorporate the entire eruption and also recognise any pre-cursory signals that may have occurred from 09/01/20 to 12/01/20. This approach would also allow a better analysis regarding the observational reports and would help support any arguments made throughout the existing research within this thesis.

A calculation error regarding TROPOMI is the cloud coverage on the days of the eruption. Cloud coverage was moderate-high for both days at 55% on 12/01/20 and 46% on 13/01/20. SO_2 underneath the cloud cover is difficult to detect using TROPOMI, therefore there is strong possibility of there being an underestimation of SO_2 using satellite monitoring. The rate of wet deposition via oxidation of SO_2 into SO_4^{2-} is increased with cloud coverage also leading to an underestimation of SO_2. From the results, it can be assumed the cloud coverage was relatively low in altitude due to the high success rate of returned pixels, but in order to validate the results these would have to be compared with other ground-based approaches. These have not been publicly provided so the data received from TROPOMI within this study should be handled with caution. Another calculation error comes from calculating the total SO_2 mass, SO_2 emission rate, MER, and $S_{content}$ in pre-eruptive melt for the 13/01/20 due to

the swath edge. The swath edge cuts off the SO_2 that has been dispersed downwind west of Taal. Consequently, an underestimation of SO_2 is highly probable. However, the bulk of the plume was within the swath boundaries.

My future recommendations include a push in creating an openly accessible global directory using TROPOMI with PlumeTraj for satellite-based monitoring combined with geophysical ground-based observations of thermal emission, deformation, and tremor in order to understand volcanic activity and aid in the detection of eruption precursors. I also believe that TROPOMI combined with PlumeTraj is a formidable software capable of producing reconstructed SO_2 time series which aids in the understanding of volcanic degassing pre- and post-eruption within the most remote volcanic regions of the world.

Chapter 7. Conclusion

The research within this thesis aimed to use TROPOMI data combined with the newly developed PlumeTraj toolkit to obtain SO_2 information of an explosive eruptive event and long-term degassing trends across the Philippine Mobile Belt and Indonesian Sangihe and Halmahera arc system. In order to achieve the aim, a series of questions were created to bring us closer to the understanding of using satellite imagery for difficult-to-access, remote volcanoes across the region. The central questions for this research were as followed:

1. What was the gas emissions associated with the Taal eruption, in terms of flux through time, total S release, injection altitude, and estimated magmatic $S_{content}$?
2. What was the nature of SO_2 emissions from Taal in the pre- and post-eruptive intervals, and how did this compare to other active volcanoes in the region?
3. Overall, what insights can we gain into volcanic processes from examining these results?

The aims of the research were to produce two sets of data: an SO_2 flux and injection altitude time series for the January 2020 eruption and to create a daily SO_2 emission per month (t day^{-1}) profile for each volcano of interest within the study period. TROPOMI provided the SO_2 data for these datasets, though application of PlumeTraj and the averaging approach allowed the creation of a reconstructed SO_2 flux times series for Taal during the 12/01/20 and daily SO_2 emission rates (t day^{-1}) for 5 well- and poorly-monitored volcanoes across the Philippine and Indonesia arcs. My findings found that there was a significantly higher $S_{content}$ within the

pre-eruptive melt (550.37 ppm) than the post-eruptive melt (91.77 ppm) indicating a singular magmatic injection increasing heat and gas pressure causing the phreatic eruption seen at approximately 13:00 PHT 12/01/20. Injection altitude caused from the explosion was recorded at three separate heights: 2.5 km, 12.8 km, and 18 km. The bulk of SO_2 detected using my methodology was found between the heights 11-13 km during both days. Using the averaging approach, estimations for the daily SO_2 emission rates per month across all 5 volcanoes (Taal, Mayon, Kanlaon, Dukono, and Karangetang) were calculated from June 2018 to February 2022, allowing a visual insight into the trend of degassing which generally coincides with the observational reports and activity seen from the volcanoes during the same period. Overall, both techniques were critical in obtaining a greater understanding of using TROPOMI combined the PlumeTraj toolkit for remote satellite sensing.

This research has shown the importance of using satellite remote sensing and the different applications that can be used to obtain varied datasets critical to aiding our understanding of eruption dynamics during pre- and post-eruptive events. In conclusion, using TROPOMI with PlumeTraj provides insights not only into quiescent degassing, but plume detection during an explosive event. Once detected, we can reconstruct the emission rates with corresponding plume height and gas flux. Satellite monitoring is a tool better equipped for strongly degassing or explosively generated plumes, which can provide difficult for ground-based monitoring operations. However, satellite monitoring has limitations when it comes to weak, low altitude plumes, in which ground-based monitoring operations can aid to quantify volatile outputs. It is vital in creating a partnership between the two approaches to increase our understanding of volcanic quiescent and eruptive degassing. Future research within remote satellite sensing should push to developing a global directory using a combination of satellite remote sensing (TROPOMI with PlumeTraj) and geophysical observations of thermal emission, deformation, and tremor in order to understand volcanic activity and contribute towards research of detecting eruption precursors.

Chapter 8. References

ABS-CBN News (2020) *Dr. Renato Solidium, Jr. gives information about Taal Volcano | Magandang Buhay, YouTube*. ABS-CBN. Available at: https://www.youtube.com/watch?v=j6zFMRd21vg

ABS-CBN News (2021) *Pure coincidence: PHIVOLCS says no connection between Kanlaon, Mayon, Taal volcanic activities.* ABS-CBN. Available at: https://news.abs-cbn.com/news/02/22/21/pure-coincidence-phivolcs-says-no-connection-between-kanlaon-mayon-taal-volcanic-activities

Acocella, V. (2014) "Great challenges in volcanology: How does the volcano factory work?," *Frontiers in Earth Science*, 2. Available at: https://doi.org/10.3389/feart.2014.00004.

Ali-Khodja, H. and Kebabi, B. (1998) "Assessment of wet and dry deposition of so attributable to a sulfuric acid plant at Annaba, Algeria," *Environment International*, 24(7), pp. 799–807. Available at: https://doi.org/10.1016/s0160-4120(98)00059-2.

Anantrasirichai, N. *et al.* (2019) "A deep learning approach to detecting volcano deformation from satellite imagery using synthetic datasets," *Remote Sensing of Environment*, 230, p. 111179. Available at: https://doi.org/10.1016/j.rse.2019.04.032.

Andres, R.J. and Kasgnoc, A.D. (1998) "A Time-averaged inventory of subaerial volcanic sulfur emissions," *Journal of Geophysical Research: Atmospheres*, 103(D19), pp. 25251–25261. Available at: https://doi.org/10.1029/98jd02091.

Arellano-Baeza, A.A., Zverev, A.T. and Malinnikov, V.A. (2006) "Study of changes in the lineament structure, caused by earthquakes in South America by applying the lineament analysis to the Aster (terra) Satellite Data," *Advances in Space Research*, 37(4), pp. 690–697. Available at: https://doi.org/10.1016/j.asr.2005.07.068.

Arpa, M.C. *et al.* (2013) "Geochemical evidence of magma intrusion inferred from diffuse CO2 emissions and Fumarole Plume Chemistry: The 2010–2011 volcanic unrest at Taal Volcano, Philippines," *Bulletin of Volcanology*, 75(10). Available at: https://doi.org/10.1007/s00445-013-0747-9.

ARTIGOS (2023) *Subduction tectonics of the Philippines*, *Artigos.wiki*. Available at: https://artigos.wiki/summary/en/Subduction_tectonics_of_the_Philippines (Accessed: April 26, 2023).

Aubry, G.J., Sator, N. and Guillot, B. (2013) "Vesicularity, bubble formation and noble gas fractionation during MORB degassing," *Chemical Geology*, 343, pp. 85–98. Available at: https://doi.org/10.1016/j.chemgeo.2013.02.006.

Audley-Charles, M.G., Ballantyne, P.D. and Hall, R. (1988) "Mesozoic-cenozoic rift-drift sequence of Asian fragments from Gondwanaland," *Tectonophysics*, 155(1-4), pp. 317–330. Available at: https://doi.org/10.1016/0040-1951(88)90272-7.

Auker, M.R. *et al.* (2013) "A statistical analysis of the Global Historical Volcanic Fatalities Record," *Journal of Applied Volcanology*, 2(1). Available at: https://doi.org/10.1186/2191-5040-2-2.

Aurelio, M.A. (2008) “Shear partitioning in the Philippines: Constraints from Philippine Fault and Global Positioning System Data,” *Island Arc*, 9(4), pp. 584–597. Available at: https://doi.org/10.1111/j.1440-1738.2000.00304.x.

Bachmeier, S (2020) *Eruption of the Taal Volcano in the Philippines.* CIMSS Satellite Blog. https://bit.ly/3sm17Nn

Balangue-Tarriela, M.I. *et al.* (2022) “Analysis of the 2020 Taal Volcano tephra fall deposits from crowdsourced information and field data,” *Bulletin of Volcanology*, 84(3). Available at: https://doi.org/10.1007/s00445-022-01534-y.

Bani, P. *et al.* (2017) “Dukono, the predominant source of volcanic degassing in Indonesia, sustained by a depleted Indian-MORB,” *Bulletin of Volcanology*, 80(1). Available at: https://doi.org/10.1007/s00445-017-1178-9.

Bartel, B.A. *et al.* (2003) “Dynamics of active magmatic and hydrothermal systems at Taal Volcano, Philippines, from continuous GPS measurements,” *Journal of Geophysical Research: Solid Earth*, 108(B10). Available at: https://doi.org/10.1029/2002jb002194.

Bato, M.G. *et al.* (2020) “The 2020 eruption and the large lateral dike emplacement at Taal Volcano, Philippines: Insights from Radar Satellite Data.” Available at: https://doi.org/10.1002/essoar.10504404.1.

Besana, G.M. *et al.* (1995) “The shear wave velocity structure of the crust and uppermost mantle beneath Tagaytay, Philippines inferred from receiver function analysis,” *Geophysical Research Letters*, 22(23), pp. 3143–3146. Available at: https://doi.org/10.1029/95gl03319.

Bignami, C. *et al.* (2012) “Ground Based Monitoring ,” *Handbook for Volcanic Risk Management Prevention, Crisis Management, Resilience* , pp. 53–70.

Bottinga, Y. and Javoy, M. (1990) “MORB degassing: Bubble growth and ascent,” *Chemical Geology*, 81(4), pp. 255–270. Available at: https://doi.org/10.1016/0009-2541(90)90050-h.

Burton, M. *et al.* (2021) “Insights into the 9 December 2019 eruption of Whakaari/White Island from analysis of tropomi so 2 imagery,” *Science Advances*, 7(25). Available at: https://doi.org/10.1126/sciadv.abg1218.

Callmander, M.W. *et al.* (2015) “The genus pandanus parkinson (Pandanaceae) on Halmahera Island (Moluccas, Indonesia) with descriptions of three new species and a key to the species on the Island,” *Candollea*, 70(2), pp. 179–195. Available at: https://doi.org/10.15553/c2015v702a2.

Camacho, A.G. *et al.* (2007) “Interpretation of 1992–1994 gravity changes around Mayon Volcano, Philippines, using Point Sources,” *Pageoph Topical Volumes*, pp. 733–749. Available at: https://doi.org/10.1007/978-3-7643-8417-3_7.

Campion, R. (2014) “New Lava Lake at Nyamuragira Volcano revealed by combined Aster and OMI SO2measurements,” *Geophysical Research Letters*, 41(21), pp. 7485–7492. Available at: https://doi.org/10.1002/2014gl061808.

Cape, J.N., Methven, J., and Hudson, L.E. (2000) “The use of trajectory cluster analysis to interpret trace gas measurements at Mace Head, Ireland,” *Atmospheric Environment*, 34(22), pp. 3651–3663. Available at: https://doi.org/10.1016/s1352-2310(00)00098-4.

Carey, S. and Burski, M. (2015) “Volcanic Plumes,” in T.Plank (ed). *The Encyclopedia of Volcanoes,* 2nd edn. ELSEVIER, pp. 571-585

Carn, S.A. *et al.* (2017) “A decade of global volcanic SO2 emissions measured from space,” *Scientific Reports*, 7(1). Available at: https://doi.org/10.1038/srep44095.

Carn, S.A. *et al.* (2021) “Advances in UV satellite monitoring of volcanic emissions,” *2021 IEEE International Geoscience and Remote Sensing Symposium IGARSS* [Preprint]. Available at: https://doi.org/10.1109/igarss47720.2021.9554594.

Carn, S.A. and Oppenheimer, C. (2000) “Remote monitoring of Indonesian volcanoes using satellite data from the internet,” *International Journal of Remote Sensing*, 21(5), pp. 873–910. Available at: https://doi.org/10.1080/014311600210344.

Castillo, P.R. and Newhall, C.G. (2004) “Geochemical constraints on possible subduction components in lavas of Mayon and Taal Volcanoes, Southern Luzon, Philippines,” *Journal of Petrology*, 45(6), pp. 1089–1108. Available at: https://doi.org/10.1093/petrology/egh005.

Clark, R.H. *et al.* (1979) “Magmatic eruption of White Island Volcano, New Zealand, December 1976–April 1977,” *New Zealand Journal of Geology and Geophysics*, 22(2), pp. 175–190. Available at: https://doi.org/10.1080/00288306.1979.10424217.

Cofano, A. *et al.* (2021) “Exploiting sentinel-5p tropomi and ground sensor data for the detection of volcanic SO2 plumes and activity in 2018–2021 at Stromboli, Italy,” *Sensors*, 21(21), p. 6991. Available at: https://doi.org/10.3390/s21216991.

Compernolle, S. *et al.* (2021) “Validation of sentinel-5p tropomi cloud data with ground-based cloudnet and other Satellite Data Products.” Available at: https://doi.org/10.5194/egusphere-egu21-5811.

Constantinescu, R. *et al.* (2021) “The radius of the umbrella cloud helps characterize large explosive volcanic eruptions,” *Communications Earth & Environment*, 2(1). Available at: https://doi.org/10.1038/s43247-020-00078-3.

Coppola, D. *et al.* (2015) “Magma extrusion during the Ubinas 2013–2014 eruptive crisis based on satellite thermal imaging (MIROVA) and ground-based monitoring,” *Journal of Volcanology and Geothermal Research*, 302, pp. 199–210. Available at: https://doi.org/10.1016/j.jvolgeores.2015.07.005.

Coppola, D. *et al.* (2019) “Monitoring the time-averaged discharge rates, volumes and emplacement style of large lava flows by using Mirova system: The case of the 2014-2015 eruption at Holuhraun (Iceland),” *Annals of Geophysics*, 61(Vol 61 (2018). Available at: https://doi.org/10.4401/ag-7749.

Coppola, D. *et al.* (2020) “Thermal Remote Sensing for Global Volcano Monitoring: Experiences from the mirova system,” *Frontiers in Earth Science*, 7. Available at: https://doi.org/10.3389/feart.2019.00362.

Corradini, S., Merucci, L. and Prata, A.J. (2009) “Retrieval of SO2 from thermal infrared satellite measurements: Correction procedures for the effects of volcanic ash,” *Atmospheric Measurement Techniques*, 2(1), pp. 177–191. Available at: https://doi.org/10.5194/amt-2-177-2009.

Daag, A.S. *et al.* (1996) "Monitoring sulphur dioxide emissions at mount Pinatubo, philippines ," *A Volatile System* [Preprint].

Dailey, I.M. (1912) "Report of the eruption of Katmai Volcano," *Bulletin of the American Geographical Society*, 44(9), p. 641. Available at: https://doi.org/10.2307/200811.

Delmelle, P. *et al.* (1998) "Geochemical and isotopic evidence for seawater contamination of the hydrothermal system of Taal Volcano, Luzon, the Philippines," *Bulletin of Volcanology*, 59(8), pp. 562–576. Available at: https://doi.org/10.1007/s004450050210.

Delmelle, P. *et al.* (2015) "Volcano Related Lakes," in T.Plank (ed.) *The Encyclopedia of Volcanoes.* 2nd edn. ELSEVIER, pp. 851-864.

Delos-Reyes, P.J. *et al.* (2018) "A synthesis and review of historical eruptions at Taal Volcano, Southern Luzon, Philippines," *Earth-Science Reviews*, 177, pp. 565–588. Available at: https://doi.org/10.1016/j.earscirev.2017.11.014.

DuFrane, S.A. *et al.* (2006) "Subduction and melting processes inferred from U-Series, SR–Nd–pb isotope, and trace element data, Bicol and Bataan Arcs, Philippines," *Geochimica et Cosmochimica Acta*, 70(13), pp. 3401–3420. Available at: https://doi.org/10.1016/j.gca.2006.04.020.

Dzurisin, D. (2003) "A comprehensive approach to monitoring volcano deformation as a window on the eruption cycle," *Reviews of Geophysics*, 41(1). Available at: https://doi.org/10.1029/2001rg000107.

Ebmeier, S.K. *et al.* (2018) "Synthesis of global satellite observations of magmatic and volcanic deformation: Implications for volcano monitoring & the lateral extent of magmatic domains," *Journal of Applied Volcanology*, 7(1). Available at: https://doi.org/10.1186/s13617-018-0071-3.

Edmonds, M. (2008) "New geochemical insights into volcanic degassing," *Philosophical Transactions of the Royal Society A: Mathematical, Physical and Engineering Sciences*, 366(1885), pp. 4559–4579. Available at: https://doi.org/10.1098/rsta.2008.0185.

Egorov, Y. (2007) "Tsunami wave generation by the eruption of Underwater Volcano," *Natural Hazards and Earth System Sciences*, 7(1), pp. 65–69. Available at: https://doi.org/10.5194/nhess-7-65-2007.

Ehara, S. *et al.* (2005) "Change in the Thermal State in a Volcanic Geothermal Reservoir beneath an Active Fumarolic Field after the 1995 Phreatic Eruption of Kuju Volcano, Japan," *Proceedings World Geothermal Congress* [Preprint].

EM-DAT (2023) *The International Disaster Database*. Available at: https://public.emdat.be/data

Esse, B. *et al.* (2022) "Quantifying SO2 emissions from the 2021 eruption of Fagradalsfjall, Iceland, with Tropomi and Plumetraj." Available at: https://doi.org/10.5194/egusphere-egu22-11537.

Ferlito, C., Viccaro, M. and Cristofolini, R. (2009) "Volatile-rich magma injection into the feeding system during the 2001 eruption of Mt. Etna (Italy): Its role on explosive activity and change in rheology of Lavas," *Bulletin of Volcanology*, 71(10), pp. 1149–1158. Available at: https://doi.org/10.1007/s00445-009-0290-x.

Freiman, M.T. and Piketh, S.J. (2003) “Air Transport into and out of the industrial highveld region of South Africa,” *Journal of Applied Meteorology*, 42(7), pp. 994–1002. Available at: https://doi.org/10.1175/1520-0450(2003)042<0994:atiaoo>2.0.co;2.

Furtney, M.A. *et al.* (2018) “Synthesizing multi-sensor, multi-satellite, multi-decadal datasets for Global Volcano Monitoring,” *Journal of Volcanology and Geothermal Research*, 365, pp. 38–56. Available at: https://doi.org/10.1016/j.jvolgeores.2018.10.002.

Galgana, G.A. *et al.* (2014) “Geodetic observations and modelling of time-varying deformation at Taal Volcano, Philippines,” *Journal of Volcanology and Geothermal Research*, 271, pp. 11–23. Available at: https://doi.org/10.1016/j.jvolgeores.2013.11.005.

Ganci, G. *et al.* (2011) “The HOTSAT Volcano Monitoring System based on combined use of SEVIRI and Modis multispectral data,” *Annals of Geophysics*, 54(5). Available at: https://doi.org/10.4401/ag-5338.

Ganci, G. *et al.* (2012) “An emergent strategy for Volcano Hazard Assessment: From thermal satellite monitoring to lava flow modelling,” *Remote Sensing of Environment*, 119, pp. 197–207. Available at: https://doi.org/10.1016/j.rse.2011.12.021.

Geronimo-Catane, S., Corpuz, E. and Punongbayan, R. (1991) “Mayon Volcano's Past and Possible Future Eruptive Activities,” *Bullitin of the volcanological society of japan*, 36(1). Available at: https://doi.org/10.18940/kazan.36.1_133.

Gevers , T. (1940) “The 1938-39 eruption of nyamlagira volcano in the kivu district of the belgian congo.”

Global Volcanism Program | Dukono (2023) *Global Volcanism Program*. Available at: https://volcano.si.edu/volcano.cfm?vn=268010

Global Volcanism Program | Karangetang (2023) *Global Volcanism Program.* Available at: https://volcano.si.edu/volcano.cfm?vn=267020

Global Volcanism Program | Taal (2023) *Global Volcanism Program.* Available at: https://volcano.si.edu/volcano.cfm?vn=273070

Gouhier, M. *et al.* (2016) “HOTVOLC: A web-based monitoring system for volcanic hot spots,” *Geological Society, London, Special Publications*, 426(1), pp. 223–241. Available at: https://doi.org/10.1144/sp426.31.

Gouhier, M. *et al.* (2020) “Operational response to volcanic ash risks using HOTVOLC satellite-based system and MOCAGE-accident model at the Toulouse Vaac,” *Atmosphere*, 11(8), p. 864. Available at: https://doi.org/10.3390/atmos11080864.

Grainger, R.G. *et al.* (2013) “Measuring volcanic plume and ash properties from space,” *Geological Society, London, Special Publications*, 380(1), pp. 293–320. Available at: https://doi.org/10.1144/sp380.7.

Haberland, C., Bohm, M. and Asch, G. (2014) “Accretionary nature of the crust of Central and east java (Indonesia) revealed by local earthquake travel-time tomography,” *Journal of Asian Earth Sciences*, 96, pp. 287–295. Available at: https://doi.org/10.1016/j.jseaes.2014.09.019.

Hall, R. (1987) “Plate boundary evolution in the Halmahera region, Indonesia,” *Tectonophysics*, 144(4), pp. 337–352. Available at: https://doi.org/10.1016/0040-1951(87)90301-5.

Hall, R. (2012) “Late Jurassic–cenozoic reconstructions of the Indonesian region and the Indian Ocean,” *Tectonophysics*, 570-571, pp. 1–41. Available at: https://doi.org/10.1016/j.tecto.2012.04.021.

Haraguchi, S. and Ishii, T. (2006) “Transitions of magma genesis estimated by change of chemical composition of Izu-bonin arc volcanism associated with spreading of Shikoku Basin,” *American Geophysical Union* [Preprint].

Hatherton, T. and Dickinson, W.R. (1969) “The relationship between andesitic volcanism and seismicity in Indonesia, the Lesser Antilles, and other island arcs,” *Journal of Geophysical Research*, 74(22), pp. 5301–5310. Available at: https://doi.org/10.1029/jb074i022p05301.

Hayer, C.S. *et al.* (2016) “Sensitivity of omi SO2 measurements to variable eruptive behaviour at Soufrière Hills Volcano, Montserrat,” *Journal of Volcanology and Geothermal Research*, 312, pp. 1–10. Available at: https://doi.org/10.1016/j.jvolgeores.2016.01.014.

Hedelt, P. *et al.* (2019) “Sulfur dioxide layer height retrieval from sentinel-5 precursor/tropomi using FP_ILM,” *Atmospheric Measurement Techniques*, 12(10), pp. 5503–5517. Available at: https://doi.org/10.5194/amt-12-5503-2019.

Henley, R.W., and Hughes, G.O. (2016) “So 2 flux and the thermal power of volcanic eruptions,” *Journal of Volcanology and Geothermal Research*, 324, pp. 190–199. Available at: https://doi.org/10.1016/j.jvolgeores.2016.04.024.

Hennemann, F.H., Conle, O.V. and Suzuki, S. (2015) “A study of the members of the tribe Phasmatini Gray 1835 that occur within the boundaries of Wallacea Phasmatodea Phasmatidae Phasmatinae Lanceocercata Zootaxa 4008,” *Zootaxa*, 4008(1), p. 1. Available at: https://doi.org/10.11646/zootaxa.4008.1.1.

Hernández, P.A. *et al.* (2017) “The acid crater lake of Taal Volcano, Philippines: Hydrogeochemical and hydroacoustic data related to the 2010–11 volcanic unrest,” *Geological Society, London, Special Publications*, 437(1), pp. 131–152. Available at: https://doi.org/10.1144/sp437.17.

Hreinsdóttir, S. *et al.* (2014) “Volcanic plume height correlated with magma-pressure change at Grímsvötn Volcano, Iceland,” *Nature Geoscience*, 7(3), pp. 214–218. Available at: https://doi.org/10.1038/ngeo2044.

Ialongo, I. *et al.* (2020) “Comparison of tropomi/sentinel-5 precursor NO2 product with ground-based observations in Helsinki and first societal applications.” Available at: https://doi.org/10.5194/egusphere-egu2020-9963.

Iino, S. *et al.* (2018) “CNN-based generation of high-accuracy urban distribution maps utilising SAR satellite imagery for short-term change monitoring,” *International Journal of Image and Data Fusion*, 9(4), pp. 302–318. Available at: https://doi.org/10.1080/19479832.2018.1491897.

Jay, J.A. *et al.* (2013) “Volcanic hotspots of the Central and southern Andes as seen from space by Aster and MODVOLC between the years 2000 and 2010,” *Geological Society, London, Special Publications*, 380(1), pp. 161–185. Available at: https://doi.org/10.1144/sp380.1.

Kagoshima, T. *et al.* (2015) "Sulphur geodynamic cycle," *Scientific Reports*, 5(1). Available at: https://doi.org/10.1038/srep08330.

Kelman, I. and Mather, T.A. (2008) "Living with volcanoes: The Sustainable Livelihoods Approach for volcano-related opportunities," *Journal of Volcanology and Geothermal Research*, 172(3-4), pp. 189–198. Available at: https://doi.org/10.1016/j.jvolgeores.2007.12.007.

Kleipool, Q. *et al.* (2018) "Pre-launch calibration results of the TROPOMI payload on-board the sentinel-5 Precursor Satellite," *Atmospheric Measurement Techniques*, 11(12), pp. 6439–6479. Available at: https://doi.org/10.5194/amt-11-6439-2018.

Kokhanovsky, A.A. *et al.* (2007) "The influence of broken cloudiness on cloud top height retrievals using nadir observations of backscattered solar radiation in the oxygen a-band," *Journal of Quantitative Spectroscopy and Radiative Transfer*, 103(3), pp. 460–477. Available at: https://doi.org/10.1016/j.jqsrt.2006.06.003.

Kumar, V. and Singha, A. (2023) *Philippines map: Map of philippines: Collection of philippines maps, MapsofWorld.com*. Available at: https://www.mapsofworld.com/philippines/ (Accessed: April 26, 2023).

Lagmay, A.M. *et al.* (2021) "Hazardous base surges of Taal's 2020 eruption." Available at: https://doi.org/10.21203/rs.3.rs-385254/v1.

Lallemand, S.E. *et al.* (1998) "Genetic relations between the Central and southern Philippine Trench and the Sangihe Trench," *Journal of Geophysical Research: Solid Earth*, 103(B1), pp. 933–950. Available at: https://doi.org/10.1029/97jb02620.

Latsch, M. *et al.* (2022) *Intercomparison of sentinel-5p tropomi cloud products for tropospheric trace gas retrievals*, *Atmospheric Measurement Techniques*. Copernicus GmbH. Available at: https://amt.copernicus.org/articles/15/6257/2022/amt-15-6257-2022.html

Liu, X. *et al.* (2004) "Errors resulting from assuming opaque lambertian clouds in toms ozone retrieval," *Journal of Quantitative Spectroscopy and Radiative Transfer*, 85(3-4), pp. 337–365. Available at: https://doi.org/10.1016/s0022-4073(03)00231-0.

Lowry, A.R. *et al.* (2001) "GPS monitoring of crustal deformation at Taal Volcano, Philippines," *Journal of Volcanology and Geothermal Research*, 105(1-2), pp. 35–47. Available at: https://doi.org/10.1016/s0377-0273(00)00238-9.

Loyola, D.G. *et al.* (2018) "The Operational Cloud Retrieval algorithms from Tropomi on board sentinel-5 precursor," *Atmospheric Measurement Techniques*, 11(1), pp. 409–427. Available at: https://doi.org/10.5194/amt-11-409-2018.

Lu, Z. *et al.* (2010) "Ground surface deformation patterns, magma supply, and magma storage at Okmok Volcano, Alaska, from Insar Analysis: 1. intereruption deformation, 1997–2008," *Journal of Geophysical Research*, 115. Available at: https://doi.org/10.1029/2009jb006969.

Ludewig, A. *et al.* (2020) "In-flight calibration results of the TROPOMI payload on board the sentinel-5 Precursor Satellite," *Atmospheric Measurement Techniques*, 13(7), pp. 3561–3580. Available at: https://doi.org/10.5194/amt-13-3561-2020.

Macpherson, C.G. *et al.* (2003) "Geochemical evolution of magmatism in an arc-arc collision: The Halmahera and Sangihe arcs, eastern Indonesia," *Geological Society, London, Special Publications*, 219(1), pp. 207–220. Available at: https://doi.org/10.1144/gsl.sp.2003.219.01.10.

Maeda, Y. *et al.* (2015) "A phreatic explosion model inferred from a very long period seismic event at Mayon Volcano, Philippines," *Journal of Geophysical Research: Solid Earth*, 120(1), pp. 226–242. Available at: https://doi.org/10.1002/2014jb011440.

Marchese, F. *et al.* (2010) "On the exportability of robust satellite techniques (RST) for active volcano monitoring," *Remote Sensing*, 2(6), pp. 1575–1588. Available at: https://doi.org/10.3390/rs2061575.

Marzocchi, W., Newhall, C. and Woo, G. (2012) "The scientific management of volcanic crises," *Journal of Volcanology and Geothermal Research*, 247-248, pp. 181–189. Available at: https://doi.org/10.1016/j.jvolgeores.2012.08.016.

Masó Miguel Saderra (1911) *The eruption of Taal Volcano, January 30, 1911*. Manila: Bureau of printing.

Massimetti, F. *et al.* (2020) "Volcanic hot-spot detection using sentinel-2: A comparison with Modis–MIROVA thermal data series," *Remote Sensing*, 12(5), p. 820. Available at: https://doi.org/10.3390/rs12050820.

Mastin, L.G. *et al.* (2009) "A multidisciplinary effort to assign realistic source parameters to models of volcanic ash-cloud transport and dispersion during eruptions," *Journal of Volcanology and Geothermal Research*, 186(1-2), pp. 10–21. Available at: https://doi.org/10.1016/j.jvolgeores.2009.01.008.

Mattioli, G.S. *et al.* (2010) "Long term surface deformation of Soufrière Hills volcano, Montserrat from GPS geodesy: Inferences from simple elastic inverse models," *Geophysical Research Letters*, 37(19). Available at: https://doi.org/10.1029/2009gl042268.

Maximo, R.P. *et al.* (2019) "Geochemical studies of thermal waters from Kanlaon Volcano, Negros Island, Philippines," *Journal of Volcanology and Geothermal Research*, 374, pp. 39–51. Available at: https://doi.org/10.1016/j.jvolgeores.2019.02.014.

McDermott, F. *et al.* (2005) "The petrogenesis of volcanics from Mt. Bulusan and Mt. Mayon in the Bicol Arc, the Philippines," *Contributions to Mineralogy and Petrology*, 150(6), pp. 652–670. Available at: https://doi.org/10.1007/s00410-005-0042-7.

Meng, Z. *et al.* (2022) "Time series surface deformation of Changbaishan volcano based on Sentinel-1B SAR data and its geological significance," *Remote Sensing*, 14(5), p. 1213. Available at: https://doi.org/10.3390/rs14051213.

Metcalfe, I. (1988) "Origin and assembly of south-East Asian continental terranes," *Geological Society, London, Special Publications*, 37(1), pp. 101–118. Available at: https://doi.org/10.1144/gsl.sp.1988.037.01.08.

Metcalfe, I. (2013) "Gondwana dispersion and Asian accretion: Tectonic and palaeogeographic evolution of Eastern Tethys," *Journal of Asian Earth Sciences*, 66, pp. 1–33. Available at: https://doi.org/10.1016/j.jseaes.2012.12.020.

Mikilus, A. *et al.* (1991) “Geochemistry of lavas from Taal Volcano, Southwestern Luzon, Philippines: Evidence for multiple magma supply systems and mantle source heterogeneity,” *Journal of Petrology*, 32(3), pp. 593–627. Available at: https://doi.org/10.1093/petrology/32.3.593.

Mojarro, J. (2020) “1754: A friar's tale of volcano's wrath,” *The Manila Times*, 17 January.

Morales Rivera, A.M. (no date) “Comparisons between omi so2 data and ground-based SO2 measurements at Turrialba Volcano.” Available at: https://doi.org/10.37099/mtu.dc.etds/334.

Morrice, M.G. *et al.* (1983) “An introduction to the Sangihe arc: Volcanism accompanying arc—arc collision in the Molucca Sea, Indonesia,” *Journal of Volcanology and Geothermal Research*, 19(1-2), pp. 135–165. Available at: https://doi.org/10.1016/0377-0273(83)90129-4.

Morrice, M.G. and Gill, J.B. (1986) “Spatial patterns in the mineralogy of island arc magma series: Sangihe Arc, Indonesia,” *Journal of Volcanology and Geothermal Research*, 29(1-4), pp. 311–353. Available at: https://doi.org/10.1016/0377-0273(86)90050-8.

Moore, J.G., Nakamura, K. and Alcaraz, A. (1966) “The 1965 eruption of Taal Volcano,” *Science*, 151(3713), pp. 955–960. Available at: https://doi.org/10.1126/science.151.3713.955.

Moune, S., Holtz, F. and Botcharnikov, R.E. (2008) “Sulphur solubility in andesitic to basaltic melts: Implications for hekla volcano,” *Contributions to Mineralogy and Petrology*, 157(6), pp. 691–707. Available at: https://doi.org/10.1007/s00410-008-0359-0.

Mukasa, S.B., Flower, M.F.J. and Miklius, A. (1994) “The ND-, SR- and PB-isotopic character of lavas from Taal, laguna de bay and arayat volcanoes, Southwestern Luzon, Philippines: Implications for ARC magma petrogenesis,” *Tectonophysics*, 235(1-2), pp. 205–221. Available at: https://doi.org/10.1016/0040-1951(94)90024-8.

NASA, (2023) *NASA Ozone Watch: Dobson Unit Facts.* Available at: Nasa Ozone Watch: Dobson Unit facts

National Historical Commission of the Philippines (2023). Available at: https://nhcp.gov.ph/

Nishigami, K. *et al.* (1994) “Shallow crustal structure beneath taal volcano, Philippines, revealed by the 1993 seismic explosion survey,” *Bulletin of the disaster prevention research institute* [Preprint].

O'Dwyer, M. *et al.* (2003) “Real-time measurement of volcanic H2S and so2 concentrations by UV spectroscopy,” *Geophysical Research Letters*, 30(12). Available at: https://doi.org/10.1029/2003gl017246.

Pakoksung, K., Suppasri, A. and Imamura, F. (2021) “Probabilistic tsunami hazard analysis of inundated buildings following a subaqueous volcanic explosion based on the 1716 tsunami scenario in Taal Lake, Philippines,” *Geosciences*, 11(2), p. 92. Available at: https://doi.org/10.3390/geosciences11020092.

Pallister, J.S., Hoblitt, R.P. and Reyes, A.G. (1992) “A basalt trigger for the 1991 eruptions of Pinatubo Volcano?,” *Nature*, 356(6368), pp. 426–428. Available at: https://doi.org/10.1038/356426a0.

Pallister, J. and McNutt, S.R. (2015) “Synthesis of volcano monitoring,” *The Encyclopedia of Volcanoes*, pp. 1151–1171. Available at: https://doi.org/10.1016/b978-0-12-385938-9.00066-3.

Pandey, P.C. (2022) “Highlighting the role of Earth Observation Sentinel5p tropomi in monitoring volcanic eruptions: A report on Hunga Tonga, a submarine volcano,” *Remote Sensing Letters*, 13(9), pp. 912–923. Available at: https://doi.org/10.1080/2150704x.2022.2106799.

Pardini, F. *et al.* (2017) “Retrieval and intercomparison of volcanic SO2 injection height and eruption time from satellite maps and ground-based observations,” *Journal of Volcanology and Geothermal Research*, 331, pp. 79–91. Available at: https://doi.org/10.1016/j.jvolgeores.2016.12.008.

Pardini, F. *et al.* (2018) “SO2 emissions, Plume Heights and magmatic processes inferred from satellite data: The 2015 calbuco eruptions,” *Journal of Volcanology and Geothermal Research*, 361, pp. 12–24. Available at: https://doi.org/10.1016/j.jvolgeores.2018.08.001.

Pardini, F. *et al.* (2019) “Initial constraints on triggering mechanisms of the eruption of Fuego Volcano (Guatemala) from 3 June 2018 using Iasi Satellite Data,” *Journal of Volcanology and Geothermal Research*, 376, pp. 54–61. Available at: https://doi.org/10.1016/j.jvolgeores.2019.03.014.

Paton, D. *et al.* (2008) “Risk perception and volcanic hazard mitigation: Individual and Social Perspectives,” *Journal of Volcanology and Geothermal Research*, 172(3-4), pp. 179–188. Available at: https://doi.org/10.1016/j.jvolgeores.2007.12.026.

Pérez, N.M. *et al.* (2022) “Diffuse CO2 degassing precursors of the January 2020 eruption of Taal Volcano, Philippines,” *Scientific Reports*, 12(1). Available at: https://doi.org/10.1038/s41598-022-22066-7.

Perttu, A. *et al.* (2020) “Estimates of plume height from infrasound for regional volcano monitoring,” *Journal of Volcanology and Geothermal Research*, 402, p. 106997. Available at: https://doi.org/10.1016/j.jvolgeores.2020.106997.

PHIVOLCS (2020) *Taal Volcano Bulletin (update) 11 January 2020 08:00 am*, *Philippine Institute of Volcanology and Seismology*. Available at: https://www.phivolcs.dost.gov.ph/index.php/volcano-hazard/volcano-bulletin2/taal-volcano/9612-taal-volcano-bulletin-11-january-2020-8-00-a-m

PHIVOLCS (2020) *Taal Volcano Bulletin (update) 12 January 2020 02:30 pm*, *Philippine Institute of Volcanology and Seismology*. Available at: https://www.phivolcs.dost.gov.ph/index.php/volcano-hazard/volcano-bulletin2/taal-volcano/9617-taal-volcano-bulletin-12-january-2020-02-30-pm

PHIVOLCS (2020) *Taal Volcano Bulletin (update) 12 January 2020 04:00 pm*, *Philippine Institute of Volcanology and Seismology*. Available at: https://www.phivolcs.dost.gov.ph/index.php/volcano-hazard/volcano-bulletin2/taal-volcano/9618-taal-volcano-bulletin-update-12-january-2020-04-00-pm.

PHIVOLCS (2020) *Taal Volcano Bulletin (update) 12 January 2020 07:30 pm*, *Philippine Institute of Volcanology and Seismology*. Available at: https://www.phivolcs.dost.gov.ph/index.php/volcano-hazard/volcano-bulletin2/taal-volcano/9620-taal-volcano-bulletin-12-january-2020-07-30-pm

PHIVOLCS (2020) *Taal Volcano Bulletin (update) 13 January 2020 08:00 am, Philippine Institute of Volcanology and Seismology*. Available at: https://www.phivolcs.dost.gov.ph/index.php/volcano-hazard/volcano-bulletin2/taal-volcano/9625-taal-volcano-bulletin-13-january-2020-8-00-a-m

PHIVOLCS (2020) *Taal Volcano Bulletin (update) 13 January 2020 08:00 am, Philippine Institute of Volcanology and Seismology*. Available at: https://www.phivolcs.dost.gov.ph/index.php/volcano-hazard/volcano-bulletin2/taal-volcano/9636-taal-volcano-bulletin-14-january-2020-8-00-a-m

PHIVOLCS (2021) *Volcano Monitoring (alert levels), Philippine Institute of Volcanology and Seismology*. Available at: https://www.phivolcs.dost.gov.ph/index.php/volcano-hazard/volcano-alert-level (Accessed: 14 May 2023).

Pratt, W.E. (1911) "The eruption of Taal Volcano," *Bulletin of the American Geographical Society*, 43(12), p. 903. Available at: https://doi.org/10.2307/200468.

Queaño, K.L. *et al.* (2020) "Consumed tectonic plates in Southeast Asia: Markers from the Mesozoic to early Cenozoic stratigraphic units in the northern and central Philippines," *Journal of Asian Earth Sciences: X*, 4, p. 100033. Available at: https://doi.org/10.1016/j.jaesx.2020.100033.

Queißer, M. *et al.* (2019) "Tropomi enables high resolution SO2 flux observations from Mt. Etna, Italy, and beyond," *Scientific Reports*, 9(1). Available at: https://doi.org/10.1038/s41598-018-37807-w.

Rosen, P.A. *et al.* (1996) "Surface deformation and coherence measurements of Kilauea Volcano, Hawaii, from SIR-C radar interferometry," *Journal of Geophysical Research: Planets*, 101(E10), pp. 23109–23125. Available at: https://doi.org/10.1029/96je01459.

Ruth, D.C. and Costa, F. (2021) "A petrological and conceptual model of Mayon Volcano (Philippines) as an example of an open-vent volcano," *Bulletin of Volcanology*, 83(10). Available at: https://doi.org/10.1007/s00445-021-01486-9.

Sabillo, K. (2020) "PHIVOLCS cleans up ash-covered instruments, sets up new stations near Taal volcano," *ABS-CBN NEWS*, 15 January.

Santoso, I. *et al.* (2022) IOP Conf. Ser.: Earth Environ. Sci. 1109 012063

Schneider, D.J., Van Eaton, A.R. and Wallace, K.L. (2020) "Satellite observations of the 2016–2017 eruption of Bogoslof Volcano: Aviation and ash fallout hazard implications from a water-rich eruption," *Bulletin of Volcanology*, 82(3). Available at: https://doi.org/10.1007/s00445-020-1361-2.

Sevilla, W.I. *et al.* (2020) "Improved 1D velocity model and deep long-period earthquakes in Kanlaon Volcano, Philippines: Implications for its magmatic system," *Journal of Volcanology and Geothermal Research*, 393, p. 106793. Available at: https://doi.org/10.1016/j.jvolgeores.2020.106793.

Shinohara, H. (2008) "Excess degassing from volcanoes and its role on eruptive and intrusive activity," *Reviews of Geophysics*, 46(4). Available at: https://doi.org/10.1029/2007rg000244.

Silver, E.A. and Moore, J.C. (1978) "The Molucca Sea Collision Zone, Indonesia," *Journal of Geophysical Research: Solid Earth*, 83(B4), pp. 1681–1691. Available at: https://doi.org/10.1029/jb083ib04p01681.

Song, Y. *et al.* (2008) "Identifying anthropogenic and natural influences on extreme pollution of respirable suspended particulates in Beijing using backward trajectory analysis," *Journal of Hazardous Materials*, 154(1-3), pp. 459–468. Available at: https://doi.org/10.1016/j.jhazmat.2007.10.064.

Sparks, R. *et al.* (1997) *Volcanic Plumes*. Wiley.

Sparks, R.S., Biggs, J. and Neuberg, J.W. (2012) "Monitoring volcanoes," *Science*, 335(6074), pp. 1310–1311. Available at: https://doi.org/10.1126/science.1219485.

Sufni Hakim, A. and Hall, R. (1991) "Tertiary volcanic rocks from the Halmahera arc, Eastern Indonesia," *Journal of Southeast Asian Earth Sciences*, 6(3-4), pp. 271–287. Available at: https://doi.org/10.1016/0743-9547(91)90073-7.

Suwarsono, S. *et al.* (2021) "Spatio-temporal anomalies in surface brightness temperature preceding volcano eruptions detected by the Landsat-8 Thermal Infrared Sensor (Case Study: Karangetang volcano)," *International Journal of Remote Sensing and Earth Sciences (IJReSES)*, 18(1), p. 43. Available at: https://doi.org/10.30536/j.ijreses.2021.v18.a3465.

Taisne, B. *et al.* (2018) "Atmospheric controls on ground- and space-based remote detection of volcanic ash injection into the atmosphere, and link to early warning systems for aviation hazard mitigation," *Infrasound Monitoring for Atmospheric Studies*, pp. 1079–1105. Available at: https://doi.org/10.1007/978-3-319-75140-5_34.

Theroux, P. (2023) *Mapcarta*. Available at: https://mapcarta.com/

Theys, N. *et al.* (2017) "Sulfur dioxide retrievals from Tropomi onboard sentinel-5 precursor: Algorithm theoretical basis," *Atmospheric Measurement Techniques*, 10(1), pp. 119–153. Available at: https://doi.org/10.5194/amt-10-119-2017.

Theys, N. *et al.* (2021) "A sulfur dioxide covariance-based retrieval algorithm (COBRA): Application to Tropomi reveals new emission sources," *Atmospheric Chemistry and Physics*, 21(22), pp. 16727–16744. Available at: https://doi.org/10.5194/acp-21-16727-2021.

Theys, N. *et al.* (2022) "Improved retrieval of so2 plume height from tropomi using an iterative covariance-based retrieval algorithm," *Atmospheric Measurement Techniques*, 15(16), pp. 4801–4817. Available at: https://doi.org/10.5194/amt-15-4801-2022.

Vajda, P. *et al.* (2012) "Inversion of temporal gravity changes by the method of local corrections: A case study from Mayon Volcano, Philippines," *Journal of Volcanology and Geothermal Research*, 241-242, pp. 13–20. Available at: https://doi.org/10.1016/j.jvolgeores.2012.06.020.

Varekamp, J.C. (2015) "The chemical composition and evolution of Volcanic Lakes," *Advances in Volcanology*, pp. 93–123. Available at: https://doi.org/10.1007/978-3-642-36833-2_4.

Vicedo, R.O., Stimac, J. and Capuno, V.T. (2008) "Establishing major permeability controls in the mak-ban geothermal field, Philippines," *Transactions - Geothermal Resources Council*, 32.

Villeneuve, M. *et al.* (2001) "Geology of the Central Sulawesi Belt (Eastern Indonesia): Constraints for geodynamic models," *International Journal of Earth Sciences*, 91(3), pp. 524–537. Available at: https://doi.org/10.1007/s005310100228.

Vogel, T.A. *et al.* (2006) "Geochemistry of Silicic magmas in the Macolod Corridor, SW Luzon, Philippines: Evidence of distinct, mantle-derived, crustal sources for silicic magmas," *Contributions to Mineralogy and Petrology*, 151(3), pp. 267–281. Available at: https://doi.org/10.1007/s00410-005-0050-7.

Wagner, T. *et al.* (2008) "Dependence of cloud properties derived from spectrally resolved visible satellite observations on surface temperature," *Atmospheric Chemistry and Physics*, 8(9), pp. 2299–2312. Available at: https://doi.org/10.5194/acp-8-2299-2008.

Wallace, P.J., Edmonds, M. and Hauri, E.H. (2015) "Volatiles in Magma ," in T. Plank (ed.) *The Encyclopedia of Volcanoes*. 2nd edn. ELSEVIER, pp. 163–183.

Wang, X., Aoki, Y. and Chen, J. (2019) "Surface deformation of asama volcano, Japan, detected by time series insar combining persistent and distributed scatterers, 2014–2018," *Earth, Planets and Space*, 71(1). Available at: https://doi.org/10.1186/s40623-019-1104-9.

Wang, C. *et al.* (2022) "Assessment of the performance of Tropomi no2 and SO2 Data Products in the north china plain: Comparison, correction and application," *Remote Sensing*, 14(1), p. 214. Available at: https://doi.org/10.3390/rs14010214.

WeatherSpark (2020) *Manila January Weather, Average Temperature (Philippines) - Weather Spark*. Available at: https://weatherspark.com/m/134588/1/Average-Weather-in-January-in-Manila-Philippines#Figures-CloudCover (Accessed: February 7, 2023).

Webster, H.N. *et al.* (2012) "Operational prediction of ash concentrations in the distal volcanic cloud from the 2010 eyjafjallajökull eruption," *Journal of Geophysical Research: Atmospheres*, 117(D20). Available at: https://doi.org/10.1029/2011jd016790.

Wessels, R.L. *et al.* (2013) "High-resolution satellite and airborne thermal infrared imaging of precursory unrest and 2009 eruption at Redoubt Volcano, Alaska," *Journal of Volcanology and Geothermal Research*, 259, pp. 248–269. Available at: https://doi.org/10.1016/j.jvolgeores.2012.04.014.

Wright, R., Carn, S.A. and Flynn, L.P. (2005) "A satellite chronology of the May–June 2003 eruption of Anatahan Volcano," *Journal of Volcanology and Geothermal Research*, 146(1-3), pp. 102–116. Available at: https://doi.org/10.1016/j.jvolgeores.2004.10.021.

Wright, R., Blackett, M. and Hill-Butler, C. (2015) "Some observations regarding the thermal flux from Earth's erupting volcanoes for the period of 2000 to 2014," *Geophysical Research Letters*, 42(2), pp. 282–289. Available at: https://doi.org/10.1002/2014gl061997.

Yamaya, Y. *et al.* (2013) "A large hydrothermal reservoir beneath Taal Volcano (Philippines) revealed by Magnetotelluric resistivity survey: 2d resistivity modelling," *Bulletin of Volcanology*, 75(7). Available at: https://doi.org/10.1007/s00445-013-0729-y.

Young, S.R. *et al.* (1998) "Overview of the eruption of Soufriere Hills Volcano, Montserrat, 18 July 1995 to December 1997," *Geophysical Research Letters*, 25(18), pp. 3389–3392. Available at: https://doi.org/10.1029/98gl01405.

Yumul, G.P. *et al.* (2020) "Subduction with arrested volcanism: Compressional regime in Volcanic Arc Gap Formation along East Mindanao, Philippines," *Journal of Asian Earth Sciences: X*, 4, p. 100030. Available at: https://doi.org/10.1016/j.jaesx.2020.100030.

Zhang, X.Y. *et al.* (2018) "Decadal trends in wet sulfur deposition in China estimated from OMI SO2 columns," *Journal of Geophysical Research: Atmospheres*, 123(18). Available at: https://doi.org/10.1029/2018jd028770.

Zhu, L. *et al.* (2011) "Transport pathways and potential sources of PM10 in Beijing," *Atmospheric Environment*, 45(3), pp. 594–604. Available at: https://doi.org/10.1016/j.atmosenv.2010.10.040.

Zlotnicki, J. *et al.* (2018) "The 2010 seismovolcanic crisis at Taal Volcano (Philippines)," *Earth, Planets and Space*, 70(1). Available at: https://doi.org/10.1186/s40623-018-0925-2.

Chapter 9. Appendices

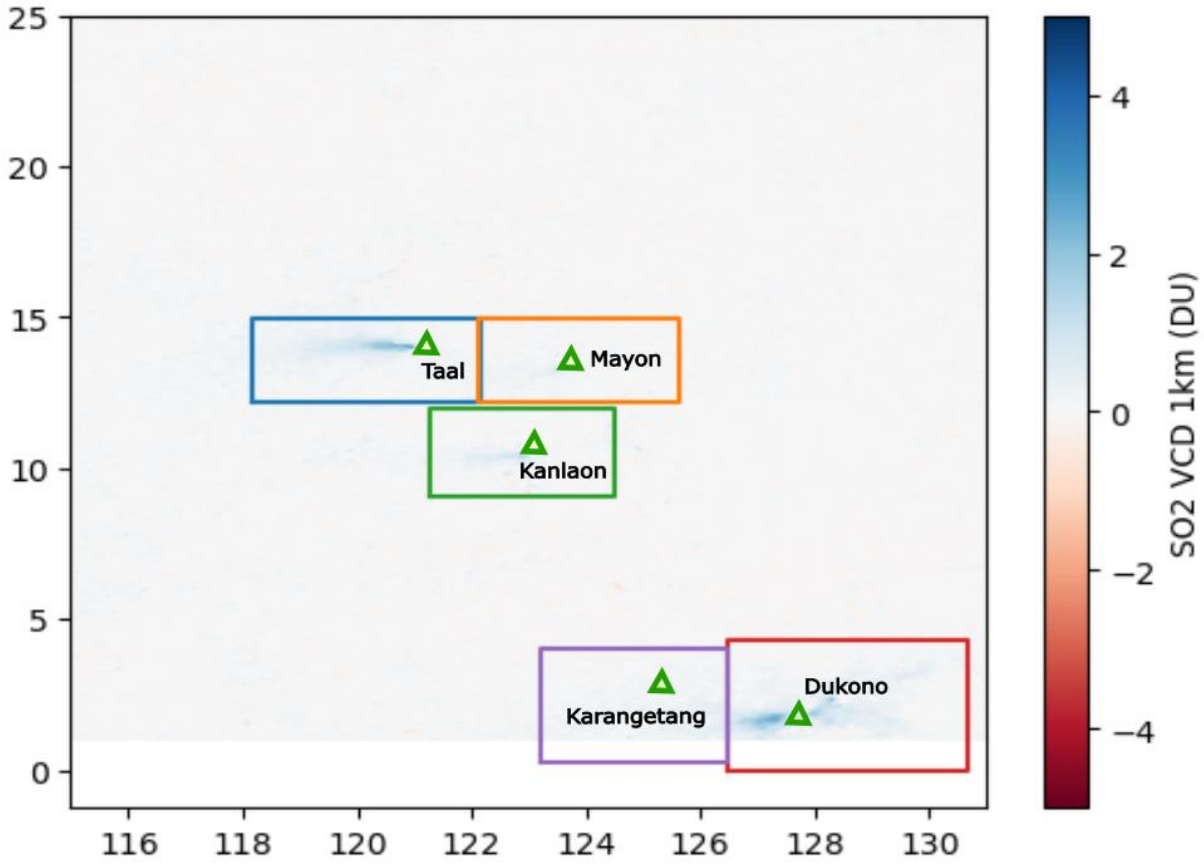

Appendix A. Visualisation of the drawn boxes used to calculate the average monthly SO_2 output (t day^{-1}) for each volcano. SO_2 VCD 1km (DU) are displayed for May 2021. Axis display latitude and longitude. Boxes for each volcano have the labelled volcano inside the perimeter.

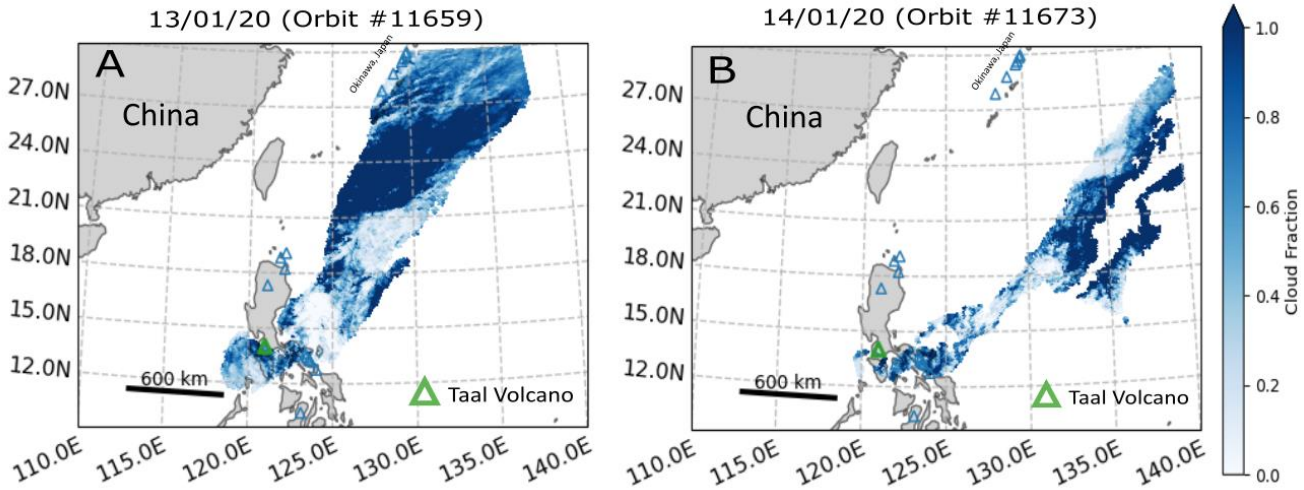

Appendix B. PlumeTraj received images using TROPOMI for January 2020 Taal eruption for 12/01/20 (left side) and 13/01/20 (right side). The figure displays vertical column densities (VCD) for 1km, 7km, and 15km used to create the corrected VCD (Figure 5.1)

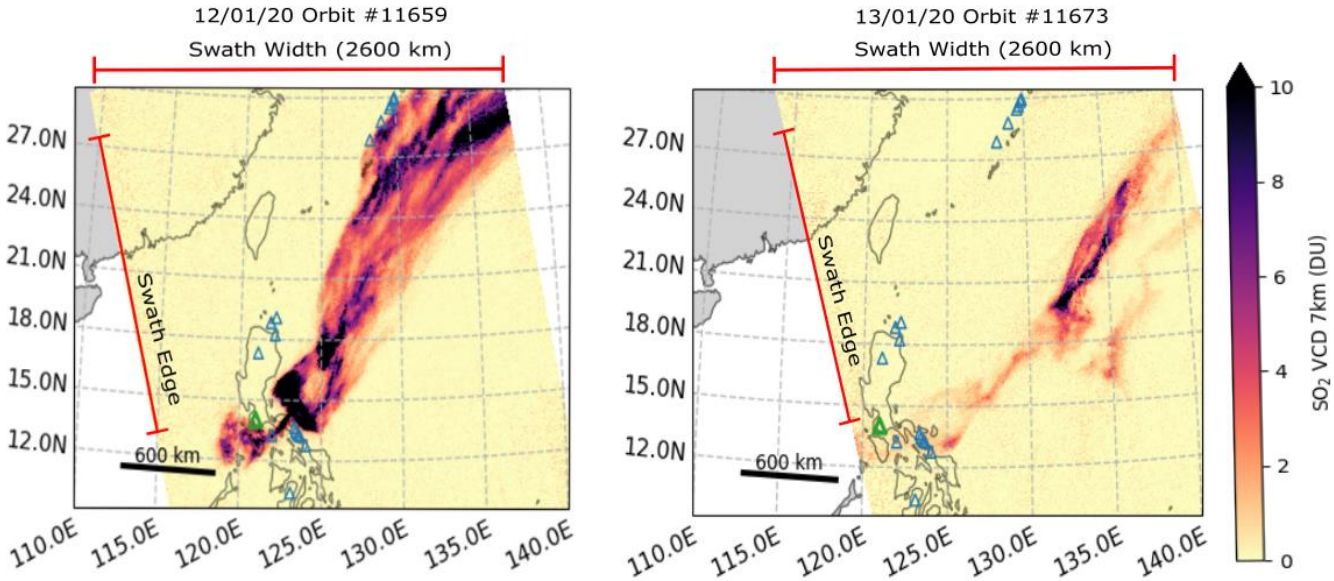

	Time	Plume Height (km)	MER (kg s^{-1})	SO_2 rate (kg/s-1)	$S_{content}$ (ppm)
12/01/20	09:00	11.5	3555801	2000	282
	10:00	12	4242712	1850	218
	11:00	12.25	4621747	2000	217
	12:00	12.4	4861177	2600	268
	13:00	12.4	4861177	2800	288
	14:00	12.6	5194924	3500	337
	15:00	12.8	5545782	6000	541
	16:00	13	5914341	5600	474
	17:00	15.3	11628156	5600	241
	18:00	15.4	11946822	3700	155
	19:00	15.3	11628156	2000	86
	20:00	12.8	5545782	1000	90
	21:00	11.9	4097900	900	110
	22:00	11.25	3245820	950	146
	23:00	10.9	2846829	2000	352
Mean		12.8	3555801	2833	254
StdDev		1.4	1990863	1711	134
13/01/20	00:00	11.5	1990863	3600	905
	01:00	10	1990863	200	50
	02:00	10	1990863	150	38
	03:00	10	2161385	100	23
	04:00	10	2956794	200	34
	05:00	10.2	4621747	280	30
	06:00	11	4621747	400	43
	07:00	12.3	5545782	400	36
	08:00	12.3	6917140	450	33
	09:00	12.8	7577739	500	33
	10:00	13.5	8044013	800	50
	11:00	13.8	8044013	1300	81
	12:00	14	8531748	1200	70
	13:00	14	4621747	1500	162
	14:00	14.2	4242712	650	77
	15:00	12.3	4590847	700	76

Appendix C. PlumeTraj received images using TROPOMI for January 2020 Taal eruption for 12/01/20 (left side) and 13/01/20 (right side) showing swath width and edge for 7 km SO_2 VCD (DU).

	16:00	12	4214346	300	36
Mean	Appendix D. All hourly values of plume height, MER, SO$_2$ emission rate, and $S_{content}$ for 12th and	12.011	3042093	571	55
StdDev	13th January 2020 Taal eruption with mean and standard deviations for both days.	1.6	2216973	430	34